



Heriot-Watt University
Research Gateway

Eulerian modelling of gas–solid flows with triboelectric charging

Citation for published version:

Kolehmainen, J, Ozel, A & Sundaresan, S 2018, 'Eulerian modelling of gas–solid flows with triboelectric charging', *Journal of Fluid Mechanics*, vol. 848, pp. 340-369. <https://doi.org/10.1017/jfm.2018.361>

Digital Object Identifier (DOI):

[10.1017/jfm.2018.361](https://doi.org/10.1017/jfm.2018.361)

Link:

[Link to publication record in Heriot-Watt Research Portal](#)

Document Version:

Peer reviewed version

Published In:

Journal of Fluid Mechanics

Publisher Rights Statement:

This article has been published in final form in *Journal of Fluid Mechanics* <https://doi.org/10.1017/jfm.2018.361>. This version is free to view and download for private research and study only. Not for re-distribution, re-sale or use in derivative works. © 2018 Cambridge University Press

General rights

Copyright for the publications made accessible via Heriot-Watt Research Portal is retained by the author(s) and / or other copyright owners and it is a condition of accessing these publications that users recognise and abide by the legal requirements associated with these rights.

Take down policy

Heriot-Watt University has made every reasonable effort to ensure that the content in Heriot-Watt Research Portal complies with UK legislation. If you believe that the public display of this file breaches copyright please contact open.access@hw.ac.uk providing details, and we will remove access to the work immediately and investigate your claim.

Eulerian Modeling of Gas-Solid Flows with Triboelectric Charging

Jari Kolehmainen¹, Ali Ozel^{1,2†}, and Sankaran Sundaresan¹

¹Department of Chemical and Biological Engineering, Princeton University, Princeton, NJ 08542, USA

²School of Engineering and Physical Sciences, Heriot-Watt University, Edinburgh EH14 4AS, UK

(Received xx; revised xx; accepted xx)

Particles subjected to flow are known to acquire electrostatic charges through repeated contacts with each other and with other surfaces. These charges alter gas-particle flow behavior at different scales. In this work, we present a continuum framework for analyzing the interplay between tribocharging and flow of monodisperse assembly of particles characterized by a single effective work function. Specifically, we have derived the continuum, kinetic theory transport equations for gas-particle flow and local-averaged charge on particles directly from the Boltzmann equation. We also derive the auxiliary conditions to capture tribocharging at bounding conducting walls. The resulting two-fluid model with tribocharging and boundary condition has then been validated against results from discrete element simulations that have been specially designed to probe specific terms in the models.

Key words: Triboelectric charging, Fluidization, Kinetic Theory, Gas-Particle Flow, Charge Transport

1. Introduction

Tendency of granular material to acquire static charges in gas-solid flows has been known for long time (Lacks & Mohan 2011). This phenomenon is known as triboelectrification or tribocharging in short. In many industrial systems, triboelectrification causes problems, such as wall sheeting in polyethylene reactors (Hendrickson 2006) and sparking in pneumatic conveying (Jones & King 1991). On the other hand, some recent applications such as triboelectric separators (Zelmat *et al.* 2013; Chen & Honaker 2015) and triboelectric generators (Fan *et al.* 2012; Kim *et al.* 2016; Wang 2017) rely on triboelectrification.

The actual charge transfer mechanisms responsible for triboelectrification are poorly understood, and multiple theories exist (Lacks & Mohan 2011). Currently the two most prominent theories are based on electron transfer (Harper 1967), and ion transfer (McCarty & Whitesides 2008). In electron transfer theory, as the name suggests, electrons are transferred between material surfaces in contact based on the electric field at contact and the difference in the work functions of the two materials. Here, the work function refers to the energy needed to remove a single electron from the material surface (Harper 1967). While the original electron transfer model (Harper 1967)

† Email address for correspondence: a.ozel@hw.ac.uk

captures the triboelectric charging of metals fairly well, it is known to perform poorly for insulating materials (Lowell & Rose-Innes 1980). This led to the notion of effective work function values as phenomenological quantities to quantify the tendency of insulators to charge (Matsusaka *et al.* 2010). Whitesides and co-workers (Wiles *et al.* 2004; McCarty *et al.* 2007) suggested that mobile ions could also be responsible for triboelectrification. This theory is supported by the fact that triboelectrification of insulators correlates well with hydrophilicity/hydrophobicity of surfaces (Schella *et al.* 2016) and that electron transfer could not explain the extent of charging in some experiments (Waitukaitis *et al.* 2014).

The most commonly used computational models for triboelectrification are based on aforementioned concept of effective work function difference or contact potential difference between surfaces (Harper 1967; Matsuyama & Yamamoto 1995; Matsusaka *et al.* 2010; Tanoue *et al.* 2001; Laurentie *et al.* 2013; Korevaar *et al.* 2014; Mizutani *et al.* 2015; Grosshans & Papalexandris 2016, 2017). Other modeling approaches described in the literature include particle polarization based charging (Pächtz *et al.* 2010; Siu *et al.* 2014; Yoshimatsu *et al.* 2016, 2017b), using particle electron surface density (Duff & Lacks 2008), high and low energy electrons (Kok & Lacks 2009), particle temperature variation based charging (Gu *et al.* 2013), and saturation charge density of the surface limited by dielectric breakdown (Korevaar *et al.* 2014). These other approaches have mostly been targeted to explain triboelectrification of particles made of the same material, when they are brought into repeated contact. In the present study, we are interested in analyzing particle charging resulting from contact with bounding surfaces made of a different material, and so we do not pursue these alternate approaches and focus on effective work function based models for triboelectrification.

Work function based model of Laurentie *et al.* (2013) has been used previously to describe triboelectrification of granular material in both gas-solid flows (Kolehmainen *et al.* 2017a) and granular systems (Laurentie *et al.* 2010; Naik *et al.* 2015, 2016; Kolehmainen *et al.* 2017b). This model takes into account the electric field at the contact point, which has been shown to impact insulator triboelectrification (Zhou *et al.* 2014; Mizutani *et al.* 2015). Furthermore, in the Laurentie *et al.* (2013) model, charge acquired by a particle following repeated contact with a wall made of different material increases linearly with the surface area of the particle, which is consistent with recent study by Chowdhury *et al.* (2018). Laurentie *et al.* (2013) found good agreement with simulations and experiments when work function values were calibrated using experimental data. Naik *et al.* (2015) used quantum chemical calculations to obtain work function values, and obtained decent agreement between the experiments and simulations of tribocharging of particles flowing in a chute. The main difference between the model by Laurentie *et al.* (2013) and other work function based models (Pei *et al.* 2013; Grosshans & Papalexandris 2016) is that Laurentie model takes into account the ambient electric field coming from many-body effects that has been shown experimentally to alter the triboelectrification (Zhou *et al.* 2014).

Electrostatic effects in both granular and gas-solid flows have been studied widely in the literature experimentally (Park & Fan 2007; Mehrotra *et al.* 2007; Sowinski *et al.* 2012; Jalalinejad *et al.* 2015; Lee *et al.* 2015; Fotovat *et al.* 2016; Yang *et al.* 2018) and also numerically (Hogue *et al.* 2008; Hassani *et al.* 2013; Yang *et al.* 2016c; Kolehmainen *et al.* 2016; Yoshimatsu *et al.* 2017a). Conducting walls attract charged particles, which has been suggested as a mechanism for wall sheeting (Hendrickson 2006). Particle charging has been found to decrease the bubble size (Jalalinejad *et al.* 2015; Hassani *et al.* 2013), and has been found to affect fine particle entrainment in circulating fluidized

beds (Fotovát *et al.* 2016; Yang *et al.* 2016*c*). For further information on the electrostatics in fluidization reader is referred to recent review paper (Fotovát *et al.* 2017).

Eulerian modeling on electrically charged gas-solid flows has been limited to predefined charges. Al-Adel *et al.* (2002) studied fully-developed gas-particle flows in vertical risers equipped with conducting walls and showed that particle charge led to lateral segregation of particles. In their analysis, the electrostatic force entered the particle-phase momentum balance as a body force. Rokkam *et al.* (2010) performed transient simulations of a two-fluid model for flow of a mixture of gas and charged particles, where electrostatic force was modeled as a body force to solid phase and the macroscopic polarization effects were accounted for by adjusting the mean electrical permittivity of the mixture. Jalalinejad *et al.* (2015, 2016) used a similar approach to model charged bubbling fluidized bed. Both Rokkam *et al.* (2013) and Jalalinejad *et al.* (2016) concluded that the model was in good agreement with the experimental results when the particle charges (treated as input parameters) were assigned appropriately.

Two-fluid model equations can be derived from the Boltzmann equation of number density function of particles by ensemble averaging. For non-rarefied flows with non-negligible amount of collisions, the collision operator accounting for the rate of change of number density function due to particle-particle collisions needs to be closed. Kinetic theory of granular flow (KTGF) achieves a closed form for the collision operator by assuming a known form for the number density function of particles (Jenkins & Savage 1983; Lun *et al.* 1984). The KTGF at early stage assumed that the particle density function followed Maxwellian velocity distribution (Jenkins & Savage 1983; Lun *et al.* 1984). More complex kinetic theories assume a perturbed Maxwellian distribution (Jenkins & Richman 1985, 1986; Boelle *et al.* 1995).

While the original kinetic theory was developed for frictionless monodisperse particles (Jenkins & Savage 1983; Lun *et al.* 1984), it has been extended to include multiple particle species (Jenkins & Mancini 1989), inter-particle cohesion (Takada *et al.* 2016), and particle friction (Lun & Savage 1987; Yang *et al.* 2016*a,b*). Kinetic theory has also been applied to heat transfer problems (Hsiau & Hunt 1993; Boateng & Barr 1996; Hunt 1997).

Charge transfer in framework of Laurentie *et al.* (2013) model is very similar to heat transfer with an exception of the electric field effect. In this work, we derive a kinetic theory based model to describe the interplay between flow and charge transfer in a mixture of gas and a mono-disperse assembly of identical particles, using the Laurentie *et al.* (2013) model for charge transfer. The ensemble averaged collision operator is decomposed into flux and source terms following Jenkins & Richman (1985). To close the resulting flux and source terms we assume Maxwellian distribution for the number density function of particles. Since, the Maxwellian based formulation is known to underestimate diffusion, we include a self-diffusion term from Hsiau & Hunt (1993) originally deduced for heat transfer. In addition, we propose a boundary condition for the particle charge at conducting solid walls and test the model and boundary condition against Discrete Element Model (DEM) simulations.

2. Theoretical Derivation

2.1. Particle Number Density Function

Let $f_p(\mathbf{x}, \mathbf{c}_p, q_p, t)$ denote number density function of particles at position \mathbf{x} with velocity \mathbf{c}_p and charge q_p on particles. Hence, number of particles with velocity between \mathbf{c}_p and $\mathbf{c}_p + d\mathbf{c}_p$ and charge between q_p and $q_p + dq_p$ at position \mathbf{x} and time t is given

by $f_p d\mathbf{c}_p dq_p$. The evolution of the particle number density function follows Boltzmann equation:

$$\frac{\partial f_p}{\partial t} + \frac{\partial}{\partial x_j} (c_{p,j} f_p) + \frac{\partial}{\partial c_{p,j}} \left(\left\langle \frac{dc_{p,j}}{dt} \middle| \mathbf{c}_p, q_p \right\rangle f_p \right) + \frac{\partial}{\partial \zeta_p} \left(\left\langle \frac{dq_p}{dt} \middle| \mathbf{c}_p, q_p \right\rangle f_p \right) = \left(\frac{\partial f_p}{\partial t} \right)_{coll} \quad (2.1)$$

where d/dt is the rate of any particle property change along the particle path due to the exchange with the fluid and the influence of resolved fields. The notation $\langle \mathcal{G} | \mathbf{c}_p, q_p \rangle$ is the expected value $\langle \mathcal{G} | c_{p,j} = C_{p,j}, q_p = \Pi_p \rangle$, and $\left(\frac{\partial f_p}{\partial t} \right)_{coll}$ is the rate of distribution function change due to particle-particle interactions.

2.2. Discrete Particle Equations

The Lagrangian approach provides a direct description of discrete phases by tracking particles of the system. By following Gatignol (1983) and Maxey (1983), the equation of motion for an isolated particle can be written as:

$$m_p \frac{dc_{p,i}}{dt} = -V_p \frac{\partial p_g}{\partial x_i} + m_p g_i - \frac{m_p}{\tau_p^*} (c_{p,i} - u_{g,i}) + F_{e,i} \quad (2.2)$$

where the first term is the instantaneous undisturbed pressure gradient at the particle centre (Archimedes force) and g_i is the acceleration due to gravity in the i^{th} direction. The third term represents the fluid-particle drag force. In Eq. (2.2), $m_p = \rho_p V_p$ is the mass of a particle; ρ_p is the particle density; V_p is the particle volume; $u_{g,i}$ is the gas velocity of the undisturbed flow. The relaxation time of a single particle τ_p^* is given by

$$\frac{1}{\tau_p^*} = \frac{3}{4} \frac{\rho_g}{\rho_p} \frac{C_D}{d_p} |\mathbf{c}_p - \mathbf{u}_g|, \quad (2.3)$$

where ρ_g is the fluid density; C_D is the drag coefficient and given by Schiller & Naumann (1935) as

$$C_D = \frac{24}{Re_p} (1 + 0.15 Re_p^{0.687}), \quad (2.4)$$

where

$$Re_p = \frac{|\mathbf{c}_p - \mathbf{u}_g| d_p}{\nu_g} \quad (2.5)$$

with the kinematic viscosity of the gas, ν_g ; and d_p is the particle diameter. Here $F_{e,i}$ is the electrostatic force that is given by

$$F_{e,i} = q_p E_i \quad (2.6)$$

where E_i is the resolved electric field and dielectrophoretic forces are neglected (LaMarche *et al.* 2010). The resolved electric field is computed by solving a Poisson's equation

$$\nabla^2 \phi = -\frac{\rho}{\epsilon} \quad (2.7)$$

for the electrical potential ϕ , where ρ is the charge density, and ϵ is the (mixture) electrical permittivity. Then, the resolved electric field is obtained by taking the gradient of the electrical potential ϕ :

$$E_i = -\nabla \phi. \quad (2.8)$$

2.3. Particle Moment Equations

The dispersed phase average of any function $\psi(\mathbf{c}_p, q_p)$ can be obtained by integrating over the particle property space as

$$\langle \psi \rangle = \frac{1}{n_p} \int_{\mathbb{R}^3} \int_{\mathbb{R}} \psi f_p dq_p d\mathbf{c}_p, \quad (2.9)$$

where n_p is the mean number of particles per unit volume, or namely particle number density given by

$$n_p(\mathbf{x}, t) = \int_{\mathbb{R}^3} \int_{\mathbb{R}} f_p dq_p d\mathbf{c}_p. \quad (2.10)$$

By definition, the mean velocity of particles is

$$U_{p,i} = \langle c_{p,i} \rangle = \frac{1}{n_p} \int_{\mathbb{R}^3} \int_{\mathbb{R}} c_{p,i} f_p d\mathbf{c}_p dq_p \quad (2.11)$$

and the fluctuating part of the disperse phase velocity is

$$c'_{p,i} = c_{p,i} - U_{p,i}. \quad (2.12)$$

The particle kinetic tensor is given by

$$\langle c'_{p,i} c'_{p,j} \rangle = \frac{1}{n_p} \int_{\mathbb{R}^3} \int_{\mathbb{R}} (c_{p,i} - U_{p,i})(c_{p,j} - U_{p,j}) f_p d\mathbf{c}_p dq_p. \quad (2.13)$$

The mean particle charge is

$$Q_p = \langle q_p \rangle = \frac{1}{n_p} \int_{\mathbb{R}^3} \int_{\mathbb{R}} q_p f_p d\mathbf{c}_p dq_p \quad (2.14)$$

and the fluctuating part of the phase charge is

$$q'_p = q_p - Q_p. \quad (2.15)$$

The charge variance is then given by

$$\langle q'_p q'_p \rangle = \frac{1}{n_p} \int_{\mathbb{R}^3} \int_{\mathbb{R}} (q_p - Q_p)^2 f_p d\mathbf{c}_p dq_p. \quad (2.16)$$

The correlations between the velocity fluctuations and the charge fluctuation are defined as

$$\langle q'_p c'_{p,i} \rangle = \frac{1}{n_p} \int_{\mathbb{R}^3} \int_{\mathbb{R}} (q_p - Q_p)(c_{p,i} - U_{p,i}) f_p d\mathbf{c}_p dq_p. \quad (2.17)$$

Enskog's general equation for the change of a function $\psi(\mathbf{c}_p, q_p)$ can be derived from the transport equation of number density function (Eq. (2.1)) by integrating over the particle property space and using the relation $n_p m_p = \alpha_p \rho_p$, where α_p is the solid phase volume fraction, as

$$\frac{\partial}{\partial t} (\alpha_p \rho_p \langle \psi \rangle) + \frac{\partial}{\partial x_i} (\alpha_p \rho_p \langle c_{p,i} \psi \rangle) = \mathcal{C}(m_p \psi) + \alpha_p \rho_p \left\langle \frac{dc_{p,i}}{dt} \frac{\partial \psi}{\partial c_{p,i}} \right\rangle + \alpha_p \rho_p \left\langle \frac{dq_p}{dt} \frac{\partial \psi}{\partial q_p} \right\rangle. \quad (2.18)$$

The mean collisional rate of change of the particle property $\mathcal{C}(m_p \psi)$ is the change of $(m_p \psi)$ due to all collisions. The particle charge is not changed by the resolved field except during the contact. Thus,

$$\frac{dq_p}{dt} = 0 \quad (2.19)$$

and the last term in Eq. (2.18) drops outs.

2.4. Mass Balance ($\psi = 1$)

The mass balance equation for solid phase is given by

$$\frac{\partial}{\partial t} (\alpha_p \rho_p) + \frac{\partial}{\partial x_i} (\alpha_p \rho_p U_{p,i}) = \mathcal{C}(m_p) \quad (2.20)$$

where $\mathcal{C}(m_p)$ represents the exchange of mass between particles during collisions due to break-up and coalescence. In this study, $\mathcal{C}(m_p) = 0$. It is also assumed in this study that there is no mass exchange between the solid and gas phases.

2.5. Momentum Balance ($\psi = u_{p,i}$)

The transport equation for solid phase momentum is given by

$$\begin{aligned} \alpha_p \rho_p \left[\frac{\partial}{\partial t} + U_{p,j} \frac{\partial}{\partial x_j} \right] U_{p,i} = & \mathcal{C}(m_p c'_{p,i}) - \frac{\partial}{\partial x_j} \left(\alpha_p \rho_p \langle c'_{p,i} c'_{p,j} \rangle \right) \\ & - \alpha_p \frac{\partial P_g}{\partial x_i} - \beta (U_{p,i} - U_{g,i}) + \frac{\alpha_p \rho_p}{m_p} Q_p E_i + \alpha_p \rho_p g_i, \end{aligned} \quad (2.21)$$

here $\beta = \alpha_p \rho_p / \tau_p$. The first two terms on the right hand side represent the rate of exchange of momentum during collisions and the rate of transport of momentum by the velocity fluctuations, respectively. They are modeled together as the divergence of a solid phase effective stress tensor: $-\partial \Sigma_{p,ij} / \partial x_j$, where

$$\Sigma_{p,ij} = \left[P_p - \lambda_p \frac{\partial U_{p,m}}{\partial x_m} \right] \delta_{ij} - \mu_p \left[\frac{\partial U_{p,j}}{\partial x_i} + \frac{\partial U_{p,i}}{\partial x_j} - \frac{2}{3} \delta_{ij} \frac{\partial U_{p,m}}{\partial x_m} \right]. \quad (2.22)$$

Assuming a Maxwellian velocity distribution, one can deduce (Ding & Gidaspow 1990) that:

$$P_p = \alpha_p \rho_p \Theta [1 + 2\alpha_p g_0 (1 + e_c)], \quad (2.23)$$

$$\mu_p = \frac{4}{5} \alpha_p^2 \rho_p d_p g_0 (1 + e_c) \sqrt{\frac{\Theta}{\pi}}, \quad (2.24)$$

and

$$\lambda_p = \frac{4}{3} \alpha_p^2 \rho_p d_p g_0 (1 + e_c) \sqrt{\frac{\Theta}{\pi}}. \quad (2.25)$$

Here, Θ is the granular temperature defined as $\Theta = \langle c'_{p,i} c'_{p,i} \rangle / 3$; e_c is the coefficient of restitution for particle-particle collisions; g_0 is the value of the radial distribution function at contact. The third and fourth terms represent the interfacial force between phases. The fifth term is the electrostatic force acting on solid phase and the last term is the gravitational force.

2.6. Transport Equation for Granular Temperature

The transport equation for granular temperature has been derived in the literature by many authors. For the assumed Maxwellian velocity distribution, one obtains (Ding & Gidaspow 1990):

$$\begin{aligned} \frac{3}{2} \frac{\partial}{\partial t} (\alpha_p \rho_p \Theta) + \frac{3}{2} \frac{\partial}{\partial x_i} (\alpha_p \rho_p U_{p,i} \Theta) = & \frac{\partial}{\partial x_i} \left(\kappa_p \frac{\partial \Theta}{\partial x_i} \right) - \Sigma_{p,ij} \frac{\partial U_{p,i}}{\partial x_j} \\ & - 12(1 - e_c^2) \frac{\alpha_p^2 \rho_p g_0}{d_p \sqrt{\pi}} \Theta^{3/2} - 3\beta \Theta. \end{aligned} \quad (2.26)$$

with the granular temperature conductivity κ_p given by

$$\kappa_p = 2\rho_p\alpha_p^2d_p(1+e_c)g_0\sqrt{\frac{\Theta}{\pi}}. \quad (2.27)$$

Derivation of the last term on the right hand side of Eq. (2.27) assumes that the fluctuations in gas and particle velocities are uncorrelated (Ding & Gidaspow 1990). Modification to this term as well as additional terms arise when these fluctuations are not uncorrelated (Koch & Sangani 1999; Gobin *et al.* 2003; Garzó *et al.* 2012). We do not consider these refinements in the present study, although one can extend the analysis to include these additional terms.

2.7. Transport Equation for Particle Charge ($\psi = q_p/m_p$)

Using Eq. (2.18), the balance equation for solid phase charge can be written as:

$$\frac{\partial}{\partial t} \left(\frac{\alpha_p \rho_p}{m_p} Q_p \right) + \frac{\partial}{\partial x_i} \left(\frac{\alpha_p \rho_p}{m_p} Q_p U_{p,i} \right) = \mathcal{C}(q_p) - \frac{\partial}{\partial x_i} \left[\frac{\alpha_p \rho_p}{m_p} \langle c'_{p,i} q'_p \rangle \right]. \quad (2.28)$$

The first term on the right hand side represents the change of charge during collisions and its analytical evaluation will be given in the next section. The second term on the right hand side represents the correlation between charge and velocity fluctuations. In this study, we limit our attention to systems where these fluctuations are essentially uncorrelated.

2.7.1. Collision Kernel for Triboelectric Charging, $\mathcal{C}(q_p)$

Following Laurentie *et al.* (2013), the rate of triboelectric charge transfer from particle i to particle j is modeled as:

$$\dot{Q}_{ij} = H \left(\frac{d\mathcal{A}_{ij}}{dt} \right) \frac{d\mathcal{A}_{ij}}{dt} \varepsilon_0 \left(\frac{\varphi_i - \varphi_j}{\delta_c e} - \mathbf{E}_{ij} \cdot \mathbf{k} \right), \quad (2.29)$$

where \mathbf{k} is the unit vector that points from particle j to particle i ; $H(\cdot)$ is Heaviside function; \mathcal{A}_{ij} is contact area between particles i and j during a collision; \mathbf{E}_{ij} is electric field at the contact point; φ_i is an effective work function of particle i ; δ_c is electron transfer cut-off distance; e is the elementary charge; ε_0 is electrical permittivity in a vacuum. Assuming that the contact area during the collision is independent of the charge transfer and the initial charge, one can solve Eq. (2.29) to obtain formula for charge transferred during the collision (see Kolehmainen *et al.* (2017a)):

$$\Delta q_{ij} = \frac{\beta_q}{\alpha_q} (1 - e^{-\alpha_q \mathcal{A}_{max}}) \approx \beta_q \mathcal{A}_{max}, \quad (2.30)$$

where α_q is geometrical quantity depending on the type of collision (Kolehmainen *et al.* 2017a), \mathcal{A}_{max} denotes the maximum contact area during the collision.

Let us consider a binary collision between mono-disperse particles $p1$ and $p2$ ($\Delta\varphi = 0$) with velocities \mathbf{c}_{p1} and \mathbf{c}_{p2} and charges q_{p1} and q_{p2} . The quantity β_q in Eq. (2.30) for particle-particle collisions is given by:

$$\beta_q = \varepsilon_0 (\mathbf{E}_{12}^+ \cdot \mathbf{k}), \quad (2.31)$$

where \mathbf{E}_{12}^+ is the total electric field given by

$$\mathbf{E}_{12}^+ = \mathbf{E}_{12} + \frac{q_{p2} - q_{p1}}{\pi \varepsilon_0 d_p^2} \mathbf{k} \quad (2.32)$$

with the resolved electric field \mathbf{E}_{12} (see Eq. (2.8)) at the contact point. The particle charges q_{p1}^+ and q_{p2}^+ after collision are given by

$$q_{p1}^+ = q_{p1} + \varepsilon_0 \mathcal{A}_{max}(\mathbf{w} \cdot \mathbf{k}) (\mathbf{E}_{12}^+ \cdot \mathbf{k}) \quad (2.33)$$

$$q_{p2}^+ = q_{p2} - \varepsilon_0 \mathcal{A}_{max}(\mathbf{w} \cdot \mathbf{k}) (\mathbf{E}_{12}^+ \cdot \mathbf{k}). \quad (2.34)$$

The maximum overlapping area $\mathcal{A}_{max}(\mathbf{w} \cdot \mathbf{k})$ can be estimated by a Hertzian collision model as given by Kolehmainen *et al.* (2017a):

$$\mathcal{A}_{max}(\mathbf{w} \cdot \mathbf{k}) = 2\pi r^* \left(\frac{15m_p^*}{32Y^* \sqrt{r^*}} \right)^{2/5} (\mathbf{w} \cdot \mathbf{k})^{4/5}, \quad (2.35)$$

where $\mathbf{w} = \mathbf{c}_{p2} - \mathbf{c}_{p1}$ is the relative velocity between particles. The effective Young's modulus, radius and mass in the above equations are defined by

$$\frac{1}{Y^*} = \frac{1 - \nu_i^2}{Y_i} + \frac{1 - \nu_j^2}{Y_j}, \quad (2.36)$$

$$\frac{1}{r^*} = \frac{1}{r_i} + \frac{1}{r_j}, \quad (2.37)$$

$$\frac{1}{m_p^*} = \frac{1}{m_{p,i}} + \frac{1}{m_{p,j}}, \quad (2.38)$$

where ν is the particle Poisson ratio.

Following Jenkins & Richman (1985), the mean collisional rate of change of charge $\mathcal{C}(q_p)$ can be written as

$$\mathcal{C}(q_p) = \int \int q_p \left(\frac{\partial f_p}{\partial t} \right)_{coll} d\mathbf{c}_p dq_p = -\frac{\partial}{\partial x_i} \theta_i(q_p) + \chi(q_p) \quad (2.39)$$

where the first term is collisional flux (representing the redistribution of q_p by particle-particle collisions) given by

$$\theta_i(q_p) = -\frac{d_p^3}{2} \int_{\mathbf{w} \cdot \mathbf{k} > 0} (q_{p1}^+ - q_{p1}) [\mathbf{w} \cdot \mathbf{k}] \mathbf{k} f_p^* d\mathbf{k} d\mathbf{c}_{p1} d\mathbf{c}_{p2} dq_{p1} dq_{p2} \quad (2.40)$$

and the second term is collisional source (representing the transfer of q_p during collisions) given by

$$\chi(q_p) = \frac{d_p^2}{2} \int_{\mathbf{w} \cdot \mathbf{k} > 0} (q_{p1}^+ - q_{p1} + q_{p2}^+ - q_{p2}) \mathbf{w} \cdot \mathbf{k} f_p^* d\mathbf{k} d\mathbf{c}_{p1} d\mathbf{c}_{p2} dq_{p1} dq_{p2}, \quad (2.41)$$

with the joint number density function f_p^*

$$f_p^* \equiv f_p^*(\mathbf{x} - \frac{d_p}{2} \mathbf{k}, \mathbf{c}_1, q_{p1}, \mathbf{x} + \frac{d_p}{2} \mathbf{k}, \mathbf{c}_2, q_{p2}, t). \quad (2.42)$$

The density function f_p^* can be written as

$$f_p^* = g_0(\alpha_p) f_{p1}(\mathbf{c}_{p1}, q_{p1}, \mathbf{x} - \frac{1}{2} d_p \mathbf{k}, t) f_{p2}(\mathbf{c}_{p2}, q_{p2}, \mathbf{x} + \frac{1}{2} d_p \mathbf{k}, t) \quad (2.43)$$

with an assumption of an uncorrelated motion of particles and g_0 is the radial distribution function at the contact (see e.g. Jenkins & Savage (1983)). Approximating the number density functions via Taylor series and ignoring higher order terms, one obtains:

$$f_p^* = g_0(\alpha_p) \left[(\alpha_p) f_{p1} f_{p2} + \frac{d_p}{2} f_{p1} f_{p2} \mathbf{k} \cdot \nabla \ln \frac{f_{p2}}{f_{p1}} \right] \quad (2.44)$$

As noted earlier, in this study we assume uncorrelated Maxwellian distribution for both velocity and charge, and write

$$f_p(\mathbf{c}_p, q_p, \mathbf{x}, t) = n_p \underbrace{\frac{1}{(2\pi\Theta_p)^{3/2}} \exp\left[-\frac{(\mathbf{c}_p - \mathbf{U}_p)^2}{2\Theta_p}\right]}_{f_{p,c}} \underbrace{\frac{1}{(2\pi\mathcal{Q}_p)^{1/2}} \exp\left[-\frac{(q_p - Q_p)^2}{2\mathcal{Q}_p}\right]}_{f_{p,q}} \quad (2.45)$$

where Θ_p is the granular temperature and \mathcal{Q}_p is the variance of charge. They are given by

$$\Theta_p = \frac{1}{3} \langle c'_{p,i} c'_{p,i} \rangle \quad (2.46)$$

$$\mathcal{Q}_p = \langle q'_p q'_p \rangle. \quad (2.47)$$

Substituting Eqs. (2.31)-(2.38) to Eqs. (2.40) and (2.41) and performing the integrations gives (see Appendix A for details):

$$\chi(q_p) = 0, \quad (2.48)$$

and

$$\theta_i(q_p) = -\sigma_q E_i(\mathbf{x}) - \kappa_q \left(\frac{\partial Q_p}{\partial x_i} - Q_p \frac{\partial \ln(Q_p)}{\partial x_i} \right), \quad (2.49)$$

where triboelectric conductivity σ_q and triboelectric diffusivity κ_q are given by

$$\sigma_q = 2^{24/5} 5\pi \sqrt{\pi} 21 \varepsilon g_0(\alpha_p) d_p^3 n_p^2 \Gamma\left(\frac{12}{5}\right) r^* \left(\frac{15m_p^*}{16Y^* \sqrt{r^*}} \right)^{2/5} \Theta_p^{9/10}, \quad (2.50)$$

and

$$\kappa_q = 2^{14/5} \frac{5\sqrt{\pi}}{21} g_0(\alpha_p) d_p^2 n_p^2 \Gamma\left(\frac{12}{5}\right) r^* \left(\frac{15m_p^*}{16Y^* \sqrt{r^*}} \right)^{2/5} \Theta_p^{9/10}, \quad (2.51)$$

where n_p is the number density given by $\alpha_p \rho_p / m_p$ and $\Gamma(\cdot)$ is the gamma function. The Soret-like term (Rahman & Saghir 2014) $Q_p \frac{\partial \ln(Q_p)}{\partial x_i}$ is generally small compared to diffusion due to gradient of the charge density, and will be neglected for the rest of this paper.

2.8. Self Diffusion of Charge

The Maxwellian distribution is known to underpredict the diffusion coefficient κ_q as it only accounts for the diffusion resulting from transfer of charge from one particle to another during contact. In reality, charge diffusion occurs through random motion of particles as well (Yang *et al.* 2016a,b), which could be captured by postulating a perturbed Maxwellian distribution. In the present study where we have limited our attention to only Maxwellian distribution, we simply add the contribution due to self-diffusion of particles derived by Hsiao & Hunt (1993) for heat conduction that takes following form in case of charge diffusion:

$$\kappa_q^* = \frac{\rho_p d_p \sqrt{\Theta}}{9\sqrt{\pi} g_0(\alpha_p)}. \quad (2.52)$$

With these modifications the charge transport equation becomes:

$$\frac{\partial}{\partial t} \left(\frac{\alpha_p}{V_p} Q_p \right) + \frac{\partial}{\partial x_i} \left(\frac{\alpha_p}{V_p} U_i Q_p \right) = \frac{\partial}{\partial x_i} (\sigma_q E_i) + \frac{\partial}{\partial x_i} \left((\kappa_q + \kappa_q^*) \frac{\partial Q_p}{\partial x_i} \right). \quad (2.53)$$

2.9. Charge Transfer Boundary Conditions

We now formulate boundary condition for charge transfer at conducting wall. Following Sakiz & Simonin (1999), the particle velocity space in the immediate vicinity of the wall is split into two subdomains: particles moving towards the wall and particles moving away from the wall:

$$D^- = \{\mathbf{c}_p \in \mathbb{R}^3 \mid c_{p,j} k_j < 0\}, \quad (2.54)$$

and

$$D^+ = \{\mathbf{c}_p \in \mathbb{R}^3 \mid c_{p,j} k_j > 0\}, \quad (2.55)$$

where \mathbf{k} is the normal vector at the wall pointing into the flow domain. The density function f_p can be also split in the same way into $f_p = f_p^+ + f_p^-$, where functions f_p^\pm are given by

$$f_p^+ = \begin{cases} f_p(\mathbf{x}, \mathbf{c}_p, q_p, t), & \text{if } \mathbf{c}_p \in D^+, \\ 0, & \text{if } \mathbf{c}_p \in D^- \end{cases} \quad \text{and} \quad (2.56)$$

$$f_p^- = \begin{cases} f_p(\mathbf{x}, \mathbf{c}_p, q_p, t), & \text{if } \mathbf{c}_p \in D^-, \\ 0, & \text{if } \mathbf{c}_p \in D^+. \end{cases} \quad (2.57)$$

The number of reflected and incident particles are obtained by

$$n_p^\pm = \int_{\mathbb{R} \times D^\pm} f_p d\mathbf{c}_p dq_p, \quad (2.58)$$

and corresponding partial averages are

$$\langle \psi \rangle^\pm = \frac{1}{n_p^\pm} \int_{\mathbb{R} \times D^\pm} \psi f_p d\mathbf{c}_p dq_p. \quad (2.59)$$

The reflected and incident density functions f_p^\pm are connected by kernel $R(\mathbf{c}^-, q_p^-, \mathbf{c}^+, q_p^+)$ that denotes the probability of incident particle with charge q_p^- and velocity \mathbf{c}_p^- to be reflected with charge q_p^+ and velocity \mathbf{c}_p^+ (Cercignani 1975):

$$f_p^+(\mathbf{x}, \mathbf{c}_p^+, q_p^+, t) |\mathbf{c}_p^+ \cdot \mathbf{k}| = \int_{\mathbb{R}^4} R(\mathbf{c}_p^-, q_p^-, \mathbf{c}_p^+, q_p^+) f_p^-(\mathbf{x}, \mathbf{c}_p^-, q_p^-, t) |\mathbf{c}_p^- \cdot \mathbf{k}| dq_p^- d\mathbf{c}_p^-. \quad (2.60)$$

As the reflected particle velocity and charge depend on only the incident quantities, we can write

$$R(\mathbf{c}_p^-, q_p^-, \mathbf{c}_p^+, q_p^+) = \delta(q_p^+ - \Lambda(\mathbf{c}_p^-, q_p^-)) \Pi \delta(\mathbf{c}_i^+ - \Psi_i(\mathbf{c}_p^-)), \quad (2.61)$$

where $\delta(\cdot)$ stands for Dirac's delta function; and $\Lambda(\cdot)$ and $\Psi(\cdot)$ are functions depending on the particle-wall interaction model. For velocity $\Psi(\cdot)$ satisfies

$$\Psi_j(\mathbf{c}_p^-) k_j = -e_w c_{p,j}^- k_j, \quad (2.62)$$

where e_w is the particle-wall restitution coefficient.

According to the model by Laurentie *et al.* (2013) the reflected charge is (analogous to Eq. (2.33))

$$\Lambda(\mathbf{c}_p^-, q_p^-) = q_p^- - \varepsilon_0 A_{max}(\mathbf{c}_p^-) \left(\frac{\Delta\varphi}{\delta_{ce}} - \frac{2q_p^-}{\pi \varepsilon_0 d_p^2} + E_{w,j} k_j \right), \quad (2.63)$$

where $\Delta\varphi$ refers to the difference in the effective work functions of the wall material and the particle, and E_w is the prevailing electric field due to all sources other than the particle under consideration. Inserting Eqs. (2.61), (2.62), and (2.63) to Eq. (2.60) gives

$$f_p^+(\mathbf{x}, \mathbf{c}_p^+, q_p^+, t) = \frac{1}{e_w J_{\Psi, \Lambda}} f_p^-(\mathbf{x}, \Psi^{-1}(\mathbf{c}_p^+), \Lambda^{-1}(\Psi^{-1}(\mathbf{c}_p^+), q_p^+), t), \quad (2.64)$$

where $J_{\Psi,\Lambda}$ is determinant of Jacobian matrix $\frac{\partial(\Psi,\Lambda)}{\partial(\mathbf{c}_p^-,q_p^-)}$. Multiplying both sides of Eq. (2.64) by $dq_p^+ d\mathbf{c}_p^+$, integrating, and invoking $n_p = n_p^+ + n_p^-$ leads to following connection between number density n_p and the incident number density n_p^- (for details see Sakiz & Simonin (1999)):

$$n_p = \frac{1 + e_w}{e_w} n_p^-. \quad (2.65)$$

Furthermore, Eq. (2.64) can be used to connect the mean quantities:

$$\begin{aligned} \langle \psi(\mathbf{c}_p, q_p) \rangle &= \frac{n_p^-}{n_p} \langle \psi(\mathbf{c}_p, q_p) \rangle^- + \frac{n_p^+}{n_p} \langle \psi(\mathbf{c}_p, q_p) \rangle^+ \\ &= \frac{e_w}{1 + e_w} \langle \psi(\mathbf{c}_p, q_p) \rangle^- + \frac{1}{1 + e_w} \langle \psi(\Psi(\mathbf{c}_p), \Lambda(\mathbf{c}_p, q_p)) \rangle^-. \end{aligned} \quad (2.66)$$

Assuming an uncorrelated Maxwellian distribution for $f_p^-(\mathbf{c}_p, q_p, \mathbf{x}, t)$ and inserting $\psi = q_p$ into the Eq. (2.66) we obtain following relation for the incident mean charge $\langle q_p \rangle^-$ and the mean charge Q_p :

$$Q_p = \langle q_p \rangle^- + \frac{\varepsilon_0 d_p \sqrt{\pi} \Gamma\left(\frac{19}{10}\right)}{2^{8/5} (1 + e_w)} \left(\frac{15 m_p}{16 Y^* \sqrt{r}} \right)^{\frac{2}{5}} \Theta^{\frac{2}{5}} \left(\frac{\Delta\varphi}{\delta_c e} - \frac{2 \langle q_p \rangle^-}{\pi \varepsilon_0 d_p^2} + E_{w,j} k_j \right). \quad (2.67)$$

To estimate the charge transfer from a wall to particles we first write:

$$\theta_i(q_p) = -\langle \Delta q \rangle^- \dot{n}_w k_i, \quad (2.68)$$

where $\langle \Delta q \rangle^-$ is the average charge transferred per collision; k_i is wall normal unit vector pointing into the flow domain; and \dot{n}_w is number of collisions per unit time per unit area. Eq. (2.68) does not account for the correlation between the transferred charge and the likelihood of particle experiencing a wall collision. We link the collision frequency to granular pressure divided by average momentum transferred to the wall by single particle:

$$\dot{n}_w = \frac{P_p}{\langle m_p c_i k_i (1 + e_w) \rangle^-} = \frac{6\sqrt{2} \alpha_p \sqrt{\Theta}}{\sqrt{\pi} (1 + e_p) d_p^3} (1 + 2(1 + e_w) \alpha_p g_0). \quad (2.69)$$

The average charge transferred by wall collision becomes:

$$\langle \Delta q \rangle^- = \frac{\varepsilon_0}{n_p^-} \int_{\mathbb{R} \times D^-} A_{max}(c_i k_i) \left(\frac{\Delta\varphi}{\delta_c e} - \frac{2q_p}{\pi \varepsilon_0 d_p^2} + E_{w,i} k_i \right) f_p dq_p d\mathbf{c}_p \quad (2.70)$$

$$= \varepsilon_0 \langle A_{max}(c_i k_i) \rangle^- \left(\frac{\Delta\varphi}{\delta_c e} - \frac{2 \langle q_p \rangle^-}{\pi \varepsilon_0 d_p^2} + E_{w,i} k_i \right) \quad (2.71)$$

$$= \varepsilon_0 \left(\frac{\sqrt{2\pi} d_p \left(\frac{15 m_p}{16 Y^* \sqrt{r}} \right)^{\frac{2}{5}} \Gamma\left(\frac{9}{10}\right)}{2^{10/5} \sqrt{2}} \Theta^{\frac{2}{5}} \right) \left(\frac{\Delta\varphi}{\delta_c e} - \frac{2 \langle q_p \rangle^-}{\pi \varepsilon_0 d_p^2} + E_{w,i} k_i \right). \quad (2.72)$$

Collecting all the terms and rearranging yields

$$\theta_i(q_p) = -\sigma_{q,w} \left(\frac{\Delta\varphi}{\delta_c e} k_i - \frac{2 \langle q_p \rangle^- k_i}{\pi \varepsilon_0 d_p^2} + E_{w,j} k_j k_i \right), \quad (2.73)$$

where triboelectric conductivity at the wall $\sigma_{q,w}$ is given by

$$\sigma_{q,w} = \varepsilon_0 \alpha_p (1 + 2(1 + e_w) \alpha_p g_0) \left(\frac{6 \left(\frac{15 m_p}{16 Y^* \sqrt{r}} \right)^{\frac{2}{5}} \Gamma\left(\frac{9}{10}\right)}{\sqrt[10]{2} (1 + e_w) d_p^2} \right) \Theta^{9/10}. \quad (2.74)$$

Equating the fluxes given by Eqs. (2.49) and (2.73), and taking dot product with the wall normal vector \mathbf{k} , yields a boundary condition for particle charge:

$$-\frac{\sigma_{q,w}}{1 - \tilde{\gamma}_q} \left(\frac{\Delta\varphi}{\delta_c e} \right) + \frac{\sigma_{q,w}}{1 - \tilde{\gamma}_q} \left(\frac{2Q_p}{\pi \varepsilon_0 d_p^2} \right) = - \left(\sigma_q - \frac{\sigma_{q,w}}{1 - \tilde{\gamma}_q} \right) E_i k_i - (\kappa_q + \kappa_q^*) \frac{\partial Q_p}{\partial x_i} k_i \quad (2.75)$$

with non-dimensional coefficient $\tilde{\gamma}_q$ being

$$\tilde{\gamma}_q = \frac{\frac{\sqrt{\pi} \Gamma\left(\frac{19}{10}\right)}{2^{3/5} (1 + e_w)} \left(\frac{15 m_p}{16 Y^* \sqrt{r}} \right)^{\frac{2}{5}} \Theta^{\frac{2}{5}}}{\pi d_p}. \quad (2.76)$$

It should be noted that assuming $\tilde{\gamma}_q \approx 0$ would be equivalent to assuming that $\langle q_p \rangle^- \equiv Q_p$. The case when $\tilde{\gamma}_q \geq 1$ describes physically a case where the particle charge transfer due to charge itself at conducting wall would be larger than the charge on particle. In context of the present model, it would require the contact area during a wall collision to become comparable with or exceed the particle surface area, which is clearly not physically possible due to geometrical constraints. Hence, $\tilde{\gamma}_q$ is much smaller than unity for real systems.

2.10. Summary of Model Equations

The model equations are cast in dimensionless form using length L , velocity U_c , density ρ_p , charge $q_{eq} = \pi \varepsilon_0 d_p^2 \Delta\varphi / (2\delta_c e)$ (Kolehmainen *et al.* 2017a) and electric potential $\phi_c = q_{eq} L^2 / (V_p \varepsilon_0)$ as characteristic quantities to obtain the following set of equations:

$$\frac{\partial \alpha_g}{\partial \tilde{t}} + \frac{\partial}{\partial \tilde{x}_j} \alpha_g \tilde{U}_{g,j} = 0 \quad (2.77)$$

$$\frac{\partial \alpha_p}{\partial \tilde{t}} + \frac{\partial}{\partial \tilde{x}_j} \alpha_p \tilde{U}_{p,j} = 0 \quad (2.78)$$

$$\frac{\partial}{\partial \tilde{t}} \alpha_g \tilde{U}_{g,i} + \frac{\partial}{\partial \tilde{x}_j} \alpha_g \tilde{U}_{g,i} \tilde{U}_{g,j} = -\frac{\rho_p}{\rho_g} \left(\alpha_g \frac{\partial \tilde{P}_g}{\partial \tilde{x}_i} - \tilde{I}_{g,i} \right) + \frac{\alpha_g \tilde{g}_i}{\text{Fr}} + \frac{1}{\text{Re}_g} \frac{\partial \tilde{\tau}_{g,ij}}{\partial \tilde{x}_j} \quad (2.79)$$

$$\tilde{\tau}_{g,ij} = \tilde{\mu}_g \left(\frac{\partial \tilde{U}_{g,i}}{\partial \tilde{x}_j} + \frac{\partial \tilde{U}_{g,j}}{\partial \tilde{x}_i} - \frac{2}{3} \delta_{ij} \frac{\partial \tilde{U}_{g,k}}{\partial \tilde{x}_k} \right) \quad (2.80)$$

$$\tilde{I}_{g,i} = \tilde{\beta} \left(\tilde{U}_{p,i} - \tilde{U}_{g,i} \right). \quad (2.81)$$

Here $\tilde{g}_i = g_i/g$; Froude number is given by $\text{Fr} = U_c^2/(gL)$; gas phase Reynolds number is defined as $\text{Re}_g = U_c L/\nu_f$; the scaled gas-particle drag coefficient is $\tilde{\beta} = L\beta/(\rho_p U_c)$; and $\tilde{\mu}_g$ is ratio of effective fluid viscosity to the actual fluid viscosity.

The non-dimensional form of particle phase momentum equation becomes

$$\frac{\partial}{\partial \tilde{t}} \alpha_p \tilde{U}_{p,i} + \frac{\partial}{\partial \tilde{x}_j} \alpha_p \tilde{U}_{p,i} \tilde{U}_{p,j} = -\alpha_p \frac{\partial \tilde{P}_g}{\partial \tilde{x}_i} + \frac{\partial \tilde{\Sigma}_{p,ij}}{\partial \tilde{x}_j} + \text{El} \alpha_p \tilde{Q}_p \tilde{E}_i + \frac{1}{\text{Fr}} \alpha_p \tilde{g}_i - \tilde{I}_{g,i}, \quad (2.82)$$

where

$$\tilde{\Sigma}_{p,ij} = -\tilde{P}_p + \tilde{\lambda}_p \frac{\partial \tilde{U}_k}{\partial \tilde{x}_k} + \tilde{\mu}_p \left(\frac{\partial \tilde{U}_i}{\partial \tilde{x}_j} + \frac{\partial \tilde{U}_j}{\partial \tilde{x}_i} - \frac{2}{3} \delta_{ij} \frac{\partial \tilde{U}_k}{\partial \tilde{x}_k} \right) \quad (2.83)$$

$$\tilde{P}_p = \alpha_p \tilde{\Theta} (1 + 2\alpha_p g_0 (1 + e_c)) \quad (2.84)$$

$$\tilde{\lambda}_p = \left(\frac{4}{3\sqrt{\pi}} \frac{d_p}{L} g_0 (1 + e_c) \right) \alpha_p^2 \sqrt{\tilde{\Theta}} \quad (2.85)$$

$$\tilde{\mu}_p = \left(\frac{4}{5\sqrt{\pi}} \frac{d_p}{L} g_0 (1 + e_c) \right) \alpha_p^2 \sqrt{\tilde{\Theta}} \quad (2.86)$$

$$(2.87)$$

and El denotes a scaled electrostatic force, referred here as the electrical inertial number, which is given by $\text{El} = q_{eq}^2 L^2 / (\varepsilon_0 \rho_p V_p^2 U_c^2)$. The electrical inertial number can be viewed as the Eulerian counterpart of the non-dimensional electrical settling velocity v_c^* introduced by Karnik & Shrimpton (2012) for charged dilute turbulent gas-particle flows. The two have a connection:

$$\text{El} \propto \frac{v_c^*}{\alpha_p}, \quad (2.88)$$

when $L = U_c / \tau_{St}$, in which τ_{St} is the Stokesian relaxation time and the U_c is the turbulent root-mean-square velocity.

The non-dimensional forms of granular temperature and charge transport equations become

$$\begin{aligned} \frac{\partial}{\partial t} \alpha_p \tilde{\Theta} + \frac{\partial}{\partial \tilde{x}_i} \alpha_p \tilde{U}_{p,i} \tilde{\Theta} &= \frac{\partial}{\partial \tilde{x}_i} \alpha_p \tilde{\kappa}_p \frac{\partial \tilde{\Theta}}{\partial \tilde{x}_i} + \tilde{\tau}_{p,ij} \frac{\partial \tilde{U}_{p,i}}{\partial \tilde{x}_j} \\ &- (3(1 - e_c^2) g_0) \alpha_p^2 \tilde{\Theta} \left(\frac{4L}{d_p} \sqrt{\frac{\tilde{\Theta}}{\pi}} - \frac{\partial \tilde{U}_{p,i}}{\partial \tilde{x}_i} \right) - 3\tilde{\beta} \tilde{\Theta}, \end{aligned} \quad (2.89)$$

$$\frac{\partial \alpha_p \tilde{Q}_p}{\partial t} + \frac{\partial \alpha_p \tilde{U}_{p,i} \tilde{Q}_p}{\partial \tilde{x}_i} = \frac{\partial}{\partial \tilde{x}_i} \tilde{\sigma}_q \tilde{E}_i + \frac{\partial}{\partial \tilde{x}_i} (\tilde{\kappa}_q + \tilde{\kappa}_q^*) \frac{\partial \tilde{Q}_p}{\partial \tilde{x}_i} \quad (2.90)$$

$$\frac{\partial^2 \tilde{\phi}}{\partial \tilde{x}_i^2} = -\alpha_p \tilde{Q}_p \quad (2.91)$$

$$\tilde{\kappa}_p = \left(\frac{g_0 (1 + e_c) \frac{d_p}{L}}{\sqrt{\pi}} \right) \alpha_p \sqrt{\tilde{\Theta}_p} \quad (2.92)$$

$$\tilde{\sigma}_q = \frac{L^2 U_c^{8/10} 2^{4/5} 5\pi \sqrt{\pi}}{V_p^2} d_p^3 \Gamma \left(\frac{12}{5} \right) \frac{r}{2} \left(\frac{15m_p}{16Y^* \sqrt{r/2}} \right)^{\frac{2}{5}} g_0 \alpha_p^2 \tilde{\Theta}_p^{9/10} \quad (2.93)$$

$$\tilde{\kappa}_q = \frac{\left(2^{-6/5} \frac{5\sqrt{\pi}}{21} d_p^2 \Gamma \left(\frac{12}{5} \right) \frac{r}{2} \left(\frac{15m_p}{16Y^* \sqrt{r/2}} \right)^{\frac{2}{5}} U_c^{8/10} \right) g_0 \alpha_p^2 \tilde{\Theta}_p^{9/10}}{LV_p} \quad (2.94)$$

$$\tilde{\kappa}_q^* = \frac{\kappa_q^*}{\rho_p U_c L}. \quad (2.95)$$

Connecting with our earlier work Kolehmainen *et al.* (2017a), the electrical inertial number can be expressed in term of $e/g = q_{eq}^2 / (m_p g) / (4\pi \varepsilon_0 d_p^2)$ ratio that described the

ratio of electrical forces at contact to gravitational force on particle and Froude number as:

$$\text{El} = 24 \left(\frac{L}{d_p} \right) \frac{e/g}{\text{Fr}}. \quad (2.96)$$

The collisional triboelectric flux at the wall can be expressed in following non-dimensional form:

$$-\tilde{\theta}_i = \tilde{\sigma}_{q,w} \left(\Delta\tilde{\varphi}k_i - \Delta\tilde{\varphi}\tilde{Q}_p k_i + \tilde{E}_j k_j k_i \right), \quad (2.97)$$

with

$$\tilde{\sigma}_{q,w} = \frac{\sigma_{q,w}L^2}{(1 - \tilde{\gamma}_q)U_c V_p \varepsilon_0}, \text{ and} \quad (2.98)$$

$$\Delta\tilde{\varphi} = \frac{8}{3} \left(\frac{d_p}{L} \right). \quad (2.99)$$

As can be seen from Eq. (2.99), the work function difference cancels out from the boundary condition due to choice of $\tilde{Q}_p = Q_p/q_{eq}$. Hence, the non-dimensional charge \tilde{Q}_p remains independent of the effective work function difference if system geometry or behavior is left unchanged. However, the electrical inertial number does depend on the work function difference, and for significantly charged systems the \tilde{Q}_p may depend on the effective work function difference in a complicated fashion (see Kolehmainen *et al.* (2017a)).

Equating the non-dimensional collisional flux at the wall to the interior flux ($-\tilde{\theta}_i = \tilde{\sigma}_q \tilde{E}_i + (\tilde{\kappa}_q + \tilde{\kappa}_q^*) \frac{\partial \tilde{Q}_p}{\partial \tilde{x}_i}$) yields boundary condition for the charge:

$$\tilde{\sigma}_{q,w} \Delta\tilde{\varphi} \left(1 - \tilde{Q}_p \right) - (\tilde{\kappa}_q + \tilde{\kappa}_q^*) \frac{\partial \tilde{Q}_p}{\partial \tilde{x}_i} k_i = (\tilde{\sigma}_q - \tilde{\sigma}_{q,w}) \tilde{E}_i k_i. \quad (2.100)$$

For very dilute flow, the contribution from macroscopic electric field becomes weaker, $\tilde{E}_i \approx 0$ and $\frac{\partial \tilde{Q}_p}{\partial \tilde{x}_i} k_i \approx 0$. With these conditions, Eq. (2.100) leads to $\tilde{Q}_p = 1$ or $Q_p = q_{eq}$ that is consistent with the definition of the equilibrium charge. Eqs. (2.90), and (2.93) to (2.100) are the new results derived in the present study.

3. Validation Test Cases

In this section, we validate constitutive relations for triboelectric conductivity σ_q , triboelectric diffusivity κ_q and the boundary condition for the charge transfer equation by using hard-sphere DEM simulation results. Details of DEM code with tribocharging are given in Appendix B. We consider two test cases; (i) transient simulations in a fully periodic domain with a specified initial spatial distribution of particle charges and (ii) steady-state charge distribution in a periodic channel bounded by conducting walls in one of the directions.

3.1. Fully Periodic Domain

To test our Eulerian charge transfer model we performed simulations in a fully periodic box with elastic particles ($d_p = 250 \mu\text{m}$, $\rho_p = 1500 \text{ kg/m}^2$, $Y = 0.5 \text{ MPa}$, $\nu = 0.42$). The box had dimensions of $192 d_p \times 12 d_p \times 12 d_p$. Simulations were performed for three different particle volume fractions: $\langle \alpha_p \rangle = 0.15$, $\langle \alpha_p \rangle = 0.25$, or $\langle \alpha_p \rangle = 0.35$. Particles were distributed homogeneously and were assigned velocities randomly, consistent with constant granular temperature $\Theta = 0.01 \text{ m}^2/\text{s}^2$ and zero mean velocity. The gas drag and electrostatic forces were neglected while solving for the motion of the particles; as

a result, the particle distribution remained homogeneous at all times, while the spatial distribution of particle charge evolved with time. As the domain-averaged electric charge is zero at all times, the macroscopic electric field obtained by solving the Poisson equation is spatially periodic in the domain. This simplified problem allows us to test the validity of the charge transfer model.

Particles were assigned initial charges:

$$Q_p(x, 0) = \begin{cases} Q_0 & \text{if } x < 96 d_p, \\ -Q_0 & \text{otherwise,} \end{cases} \quad (3.1)$$

where x is the x coordinate of the particle, and $Q_0 = 10^{-15}$ C is the initial particle charge. Due to periodicity and absence of mean convection of charge, the problem simplifies to

$$a \frac{\partial Q_p(x, t)}{\partial t} = b Q_p(x, t) + c \frac{\partial^2 Q_p}{\partial x^2}, \quad (3.2)$$

where a , b , and c are constants depending on particle properties, volume fraction, and granular temperature:

$$a = \alpha_p \rho_p, \quad (3.3)$$

$$b = -\frac{\sigma_q \alpha_p}{\varepsilon_0 V_p}, \quad (3.4)$$

$$c = \kappa_q + \kappa_q^*. \quad (3.5)$$

Equation (3.2) can be solved using sine series to obtain:

$$Q_p(x, t) = \sum_{n=1}^{\infty} \gamma_n e^{(b-c(\frac{2\pi n}{L})^2)t} \sin(\frac{2\pi n}{L}x), \quad (3.6)$$

where L is the box length, and γ_n are coefficients corresponding to initial charge distribution:

$$\gamma_n = \frac{2Q_0}{n\pi} (1 - (-1)^n). \quad (3.7)$$

The analytical solution given by Eq. (3.6) was compared against hard sphere DEM simulation results to validate the used approach.

As the value of the radial distribution function at contact g_0 has a significant impact on the charge transfer rate, we computed it directly from the actual DEM data produced by the present simulations.

3.2. Periodic Channel with Conducting Walls

To assess the validity of the boundary condition given by Eq. (2.100) we performed simulations in a periodic channel with dimensions $L \times L_p \times L_p$ where $L_p = 8 d_p$ with particle diameter $d_p = 75 \mu\text{m}$, and particle density $\rho_p = 1500 \text{ kg/m}^3$. The channel width L was varied, and we performed simulations for three different values: $64 d_p$, $128 d_p$, and $256 d_p$. Particles were frictionless and had restitution coefficient of unity, hence there was no decay of kinetic energy. For each channel width, simulations were performed for three different solid volume fractions, namely $\langle \alpha_p \rangle = 0.15$, $\langle \alpha_p \rangle = 0.25$ and $\langle \alpha_p \rangle = 0.35$, and one granular temperature $\Theta = 0.01 \text{ m}^2/\text{s}^2$. Channel walls were assumed to be made of a conducting material and were modeled with a constant electric potential boundary condition; and the work function difference between the channel walls and particles was assumed as 0.001 eV ($q_{eq} = 15.6 \text{ fC}$). Lastly, particles and the walls had the same Young's modulus of 0.5 MPa and the same Poisson ratio of 0.42 .

The particle dynamics simulations were carried out following the same hard-sphere

approach explained in the Appendix B with an exception that the channel was mirrored in the wall normal directions in order to use the spectral approach to determine the electric field. As in the test problem mentioned in Section 3, the gas drag, gravity and electrostatic force acting on the particles were neglected so that the particle distribution remained uniform; this allowed us to focus on assessing the accuracy of the charge transfer boundary condition. The mesh size for the spectral method was set to $2d_p$ in each direction. Particle dynamics simulations were continued until the total charge in the system and the charge profile had become steady, independent of time.

We solved the Eulerian model equations (Eqs. (2.90), (2.91), and (2.100)) numerically by finite difference method employing 128 mesh points in the wall normal direction. Gradients in the periodic directions and the time derivatives were ignored as our interest lies in comparing the steady state solution afforded by the Eulerian model with the results from the particle dynamics simulations. Gradient and divergence operators in the finite difference formulation were discretized by 2nd order central difference scheme, and resulting linear algebraic problem was solved using Gaussian elimination. It should be noted that even though the physical properties were specified in dimensional form, the entire problem could easily have been stated in terms of dimensionless groups; presenting an example in dimensional terms still achieves the desired the model assessment. The results in the following sections are presented in terms of dimensional quantities.

3.3. Comparison of Euler-Euler results with hard sphere DEM simulations

Fig. 1 shows both the periodic channel and box simulation results and the model predictions for 0.25 and 0.35 volume fractions. As can be seen from the figure, the developed model predictions are close to the particle dynamics simulation results for $\langle\alpha_p\rangle = 0.35$, but differ slightly for moderate volume fraction $\langle\alpha_p\rangle = 0.25$. We noted the results become exact if the triboelectric conductivity σ_q was increased by $\sim 10\%$ and $\sim 20\%$ for the volume fractions 0.35 and 0.25, respectively.

Fig. 2 shows the periodic box and periodic channel simulation results for lower volume fraction ($\langle\alpha_p\rangle = 0.15$) along with the predictions of the Eulerian model. The model predictions diverge further from DEM simulations results. It was found out that the source of difference in the results originated from underpredicting the triboelectric conductivity, for this volume fraction by $\sim 40\%$.

In the periodic domain simulations, the charge density profile remains mostly flat in each half domain, but decreases in magnitude with increasing time, with transition occurring in a relatively short distance at the boundaries of the half-domains. This pattern can readily be attributed to the dominance of the triboelectric charge conductivity term (which appears through the first term on the right hand side of Eq. (3.2)) in this validation example. This test problem provides a satisfactory validation of the model for triboelectric charge conductivity.

In the wall-bounded tribocharging example, we found that both κ_q and κ_q^* should be taken into account to capture the spatial variation of charge density. At high particle volume fractions, triboelectric charge diffusivity κ_q is more important than charge diffusion due to particle migration κ_q^* since $\kappa_q/\kappa_q^* \propto (\alpha_p g_0)^2$. At lower particle volume fractions, κ_q^* contributes more than κ_q . This test problem validates the wall boundary condition and the charge diffusivity models. Taken together, these two examples lend support to all the constitutive models proposed in this study.

Whereas the results from this study cannot be compared with any experiments directly, the higher charge observed at the wall is consistent with findings of Sowinski *et al.* (2012). In the proposed model, the charge distribution in the channel depends on the ratio of triboelectric diffusivity and triboelectric conductivity $((\kappa_q + \kappa_q^*)/\sigma_q)$. The gradient of

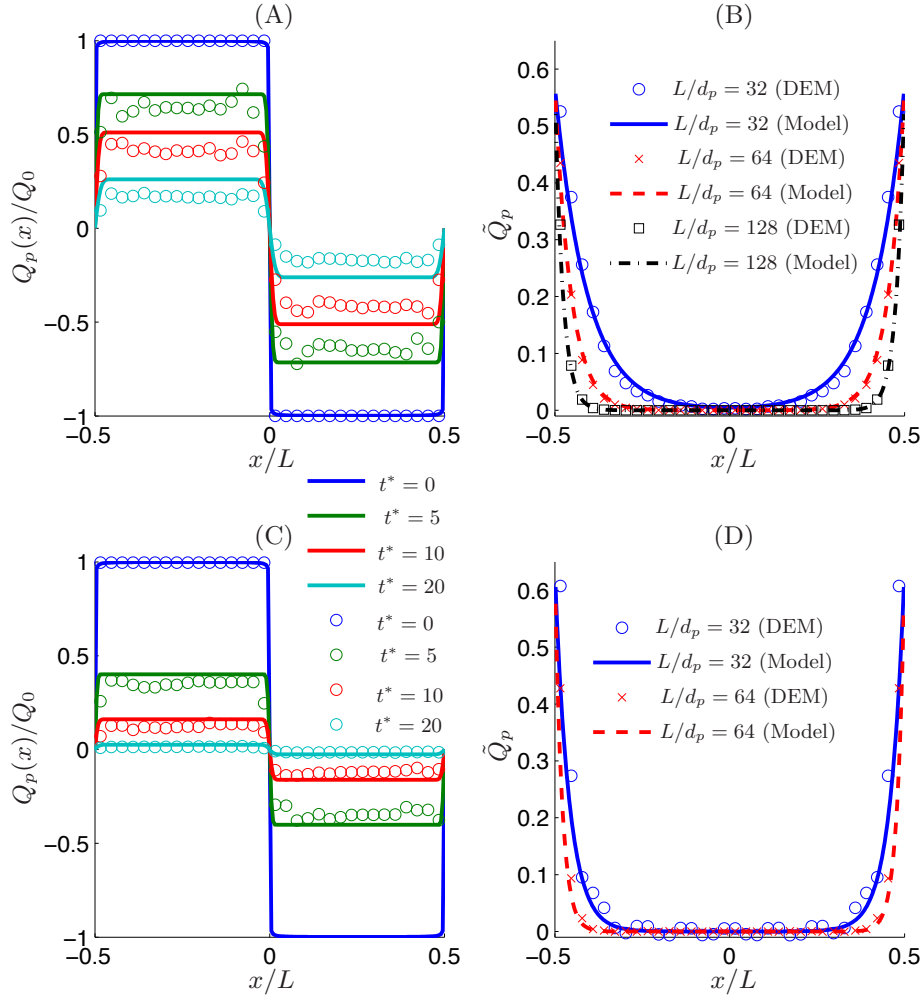


FIGURE 1. Panel (A): periodic box simulation with $\langle\alpha_p\rangle = 0.25$; Panel (B): periodic channel with $\langle\alpha_p\rangle = 0.25$; Panel (C): periodic box simulation with $\langle\alpha_p\rangle = 0.35$; and Panel (D): periodic channel with $\langle\alpha_p\rangle = 0.35$. The time for periodic box is scaled by: $t^* = t\sqrt{\Theta}/d_p$, and the charge in the beginning of the simulation is $Q_0 = \pm 10^{-15}$. The equilibrium charge for the channel simulations is $q_{eq} = 15.6$ fC. The channel width for the periodic channel simulations was varied and is given in the legend of Panels B and D. The radial distribution functions at contact were estimated from the DEM data and are 1.8 and 2.5, for $\langle\alpha_p\rangle = 0.25$ and $\langle\alpha_p\rangle = 0.35$ respectively.

charge at the wall becomes steeper as the ratio of diffusivity to conductivity decreases. In particular, when Young's modulus is decreased both κ_q and σ_q decrease at the same rate, but κ_q^* remains unchanged. Hence, for very stiff particles the charge profile would approach a flat line, variation would be confined to a thin boundary layer near the bounding wall and be uniform in the bulk.

4. Conclusions

In this study, we have derived Eulerian triboelectric charge transfer model from the Boltzmann equation and a boundary condition for charge transfer at a conducting

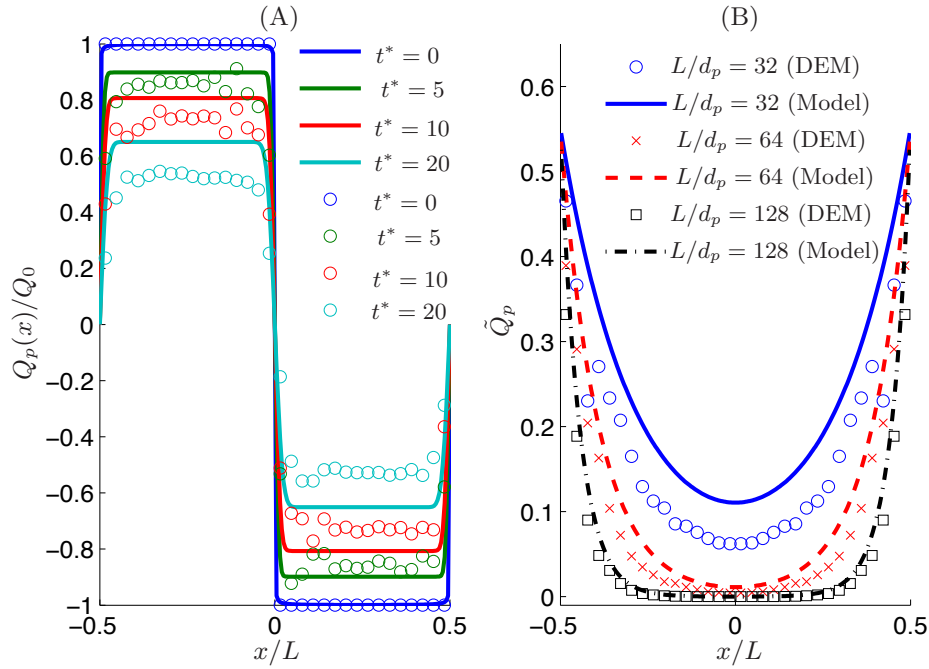


FIGURE 2. Panel (A): periodic box simulation with $\langle \alpha_p \rangle = 0.15$; and Panel (B): periodic channel with $\langle \alpha_p \rangle = 0.15$. See Fig. 1 caption for details. The radial distribution function at contact is estimated from the DEM data and is 1.6 for $\langle \alpha_p \rangle = 0.15$.

wall. The charge transfer model is closed by assuming a Maxwellian distribution for both particle charge and velocity and assuming that the two are independent. As the assumption of a Maxwellian velocity distribution is known to underestimate the diffusion coefficient, a correction is added following same reasoning presented by Hsiao & Hunt (1993).

The principal findings from the model derivation are that the combined effects of tribocharging and particle motion on charge transport can be understood through following contributions: convection, triboelectric conductivity (σ_q), triboelectric diffusion (κ_q) and charge diffusion through random motion of particles (κ_q^*). Out of these, κ_q^* is more significant than κ_q . The analysis shows that the severity of charge gradient near a boundary is determined by the ratio of triboelectric conductivity and charge diffusivity.

The derived transport equation for charge has resemblance to a scalar transport equation in granular flows such as heat transfer between solid particles with an exception of the electric field. The electric field term $\sigma_q \mathbf{E}$ can be interpreted as a triboelectric current density and exhibits a similar mathematical form to electrostatics of conductors where electric field generates a current that depends on the metals conductivity. While Zhou *et al.* (2014) has shown that an external electric field modifies the triboelectric behavior, there is no published study that measure the triboelectric current to the best of author's knowledge. It remains to be shown experimentally that an external electric field spans a current in an agitated granular material.

The proposed Eulerian model was tested against hard-sphere DEM simulations in a fully periodic box with a prescribed initial charge distribution. We also carried out hard-sphere DEM simulations in a periodic channel with conducting walls to probe the validity of the boundary condition. The charge transfer model predicted the DEM results fairly well for high volume fraction ($\langle \alpha_p \rangle = 0.35$), but differed noticeably for low volume

fraction ($\langle \alpha_p \rangle = 0.15$). The discrepancies in the results are attributed to the validity of the assumptions of Maxwellian distributions of particle charge and velocity for the low volume fraction flow regime. We have included a correction for the triboelectric charge diffusivity, but neglected the one for the triboelectric conductivity as there is no prior example for similar mechanism from other disciplines of granular mechanics.

Our analysis assumes that there is no correlation between particle charge and velocity. This assumption is justified for high volume fraction and low electric field as follows. Particle charge and momentum are redistributed in a rapid fashion due to high collision frequency, and the impulse due to the electric field has negligible effect on particle motion. However, the scenario becomes different when particle-particle collisions are not abundant and duration between sequential collisions is long. For the later case, the electrostatic force can create a significant acceleration of particles between the collisions. Hence, it can be expected that for low solid volume fractions particle charge and velocity would become correlated. The probability density function of particle velocity is also known to deviate from Maxwellian for low volume fractions, and therefore it is unlikely that the current model would work well for low volume fractions. This is also consistent with our comparisons with DEM simulations that showed increased deviation from the model predictions when solid volume fraction was decreased.

The present model accounts for electrostatic interactions between particles, but it does not take into account the effect of electrostatics on solid phase stresses. Furthermore, insulating particles exhibit dielectrophoresis (Siu *et al.* 2015) that increases particle collision frequency in the direction of the electric field. This phenomenon would lead to a non-linear relationship between the triboelectric current and the electric field as opposed to the linear relation used in this study. The charge diffusion would also become anisotropic as opposed to isotropic coefficient derived in this work. These microscopic interactions are also likely to further alter solid phase stresses and granular temperature. Additionally, the microscopic triboelectric charging model used in this study lacks some experimentally identified properties, such as tribocharging between identical particles (Lee *et al.* 2015) or particle size dependent charging (Carter & Hartzell 2017). These effects would increase the local variance of the particle charge, but in the present model charge variance affected the solution only via the Soret-like term, which was deemed negligible. Analysis of these effects will be pursued in future studies.

Although a Maxwellian form of probability density function is a reasonable assumption for homogenous cases (cases considered in this study), the distribution function is expected to be different under gradients of solid phase velocity and granular temperature. Natural extension of this study will be to deviate the Maxwellian form by using Grad's method (Jenkins & Richman 1985). For dilute gas-solid flows with tribocharging, the correlation between particle charge and velocity should be accounted for. A possible approach to model the particle velocity-charge correlation is to decompose the particle charge into correlated and uncorrelated parts by following Février *et al.* (2005) and Fox (2014), and develop mesoscopic Eulerian transport equations for the correlated part of charge. It is also necessary to develop the transport equation for charge variance (similar to transport equation for granular temperature) to account for the effect of high charge density gradient on triboelectric conductivity and diffusivity. Additionally, typical industrial applications of triboelectric charging, such as triboelectric separators used for coal separation (Blissett & Rowson 2012) or plastic waste recovery (Bendimerad *et al.* 2009), involve particles with size distribution and with different chemical and physical properties. To model such applications, the present model would need to be extended to include multiple different species similar to Jenkins & Mancini (1989).

This material is based upon work supported by the National Science Foundation Grant No. CBET-1601986 and ExxonMobil Res. & Eng. Co.

Appendix A. Analytical Derivation of Charge Transfer Collisional Kernel

The source term $\chi(q_p)$ for charge transfer vanishes since $q_{p1}^+ - q_{p1} + q_{p2}^+ - q_{p2} \equiv 0$ due to charge conservation. The flux term $\theta_i(q_p)$ can be split into two integrals:

$$\theta(q_p) = \varepsilon_0 g_0 \frac{d_p^3}{2} \theta_1(q_p) + \varepsilon_0 g_0 \frac{d_p^4}{4} \theta_2(q_p), \quad (\text{A } 1)$$

where

$$\theta_1(q_p) = \int_{\mathbf{w} \cdot \mathbf{k} > 0} \mathcal{A}_{max}(\mathbf{w} \cdot \mathbf{k}) (\mathbf{E}_{12}^+ \cdot \mathbf{k}) [\mathbf{w} \cdot \mathbf{k}] \mathbf{k} f_{p1} f_{p2} d\mathbf{k} d\mathbf{c}_{p1} d\mathbf{c}_{p2} dq_{p1} dq_{p2} \quad (\text{A } 2)$$

and

$$\theta_2(q_p) = \int_{\mathbf{w} \cdot \mathbf{k} > 0} \mathcal{A}_{max}(\mathbf{w} \cdot \mathbf{k}) (\mathbf{E}_{12}^+ \cdot \mathbf{k}) [\mathbf{w} \cdot \mathbf{k}] \mathbf{k} f_{p1} f_{p2} \mathbf{k} \cdot \nabla \ln\left(\frac{f_{p2}}{f_{p1}}\right) d\mathbf{k} d\mathbf{c}_{p1} d\mathbf{c}_{p2} dq_{p1} dq_{p2}. \quad (\text{A } 3)$$

The first integral $\theta_1(q_p)$ can be simplified as

$$\begin{aligned} \theta_1(m_p q_p) &= \int_{\mathbf{w} \cdot \mathbf{k} > 0} \mathcal{A}_{max}(\mathbf{w} \cdot \mathbf{k}) \left[\mathbf{E}_{12} \cdot \mathbf{k} + \frac{q_{p2} - q_{p1}}{\pi \varepsilon_0 d_p^2} \right] [\mathbf{w} \cdot \mathbf{k}] \mathbf{k} f_{p1} f_{p2} d\mathbf{k} d\mathbf{c}_{p1} d\mathbf{c}_{p2} dq_{p1} dq_{p2} \\ &= \frac{n_p^2}{(2\pi\Theta_p)^3} \mathbf{E}_{12} \cdot \\ &\quad \int_{\mathbf{w} \cdot \mathbf{k} > 0} (\mathbf{k} \otimes \mathbf{k}) \mathcal{A}_{max}(\mathbf{w} \cdot \mathbf{k}) [\mathbf{w} \cdot \mathbf{k}] \\ &\quad \times \exp\left[-\frac{(\mathbf{c}_{p1} - \mathbf{U}_p)^2 + (\mathbf{c}_{p2} - \mathbf{U}_p)^2}{2\Theta_p}\right] d\mathbf{k} d\mathbf{c}_{p1} d\mathbf{c}_{p2} \\ &= \frac{n_p^2}{(2\pi\Theta_p)^3} \mathbf{E}_{12} \cdot \mathbf{I}^v, \end{aligned} \quad (\text{A } 4)$$

since the charge contribution vanishes

$$\frac{1}{2\pi\mathcal{Q}} \int_{\mathbb{R} \times \mathbb{R}} \frac{q_{p2} - q_{p1}}{\pi \varepsilon_0 d_p^2} \exp\left[-\frac{(q_{p1} - Q_p)^2 + (q_{p2} - Q_p)^2}{2\mathcal{Q}_p}\right] dq_{p1} dq_{p2} = 0. \quad (\text{A } 5)$$

The remaining integral of $\theta_1(m_p q_p)$ can be integrated by changing the variables from \mathbf{c}_{p1} and \mathbf{c}_{p2} to $\mathbf{G} = \mathbf{c}_{p1} + \mathbf{c}_{p2} - 2\mathbf{U}_p$ and $\mathbf{w} = \mathbf{c}_{p1} - \mathbf{c}_{p2}$ which gives:

$$d\mathbf{c}_{p1} d\mathbf{c}_{p2} = \frac{\partial(\mathbf{c}_{p1}, \mathbf{c}_{p2})}{\partial(\mathbf{w}, \mathbf{G})} d\mathbf{w} d\mathbf{G} = \frac{1}{2} d\mathbf{w} d\mathbf{G}. \quad (\text{A } 6)$$

The inner most integration respect to \mathbf{k} can be calculated when the unit vector \mathbf{k} is expressed in spherical coordinates respect to \mathbf{w} :

$$\mathbf{k} = \begin{bmatrix} \cos \varphi' \sin \theta' \\ \sin \varphi' \sin \theta' \\ \cos \theta' \end{bmatrix}, \quad (\text{A } 7)$$

where θ' is angle between \mathbf{k} and \mathbf{w} . This yields $\mathbf{w} \cdot \mathbf{k} dk = w \cos \theta' \sin \theta' d\theta' d\varphi'$. Substituting these simplifies the $\theta_1(q_p)$ flux as:

$$\begin{aligned} \theta_1(q_p) &= \frac{n_p^2}{2(2\pi\Theta_p)^3} \mathbf{E}_{12} \cdot \int_{\mathbf{w} \cdot \mathbf{k} > 0} \mathbf{R} \Lambda \mathbf{R}^T w \mathcal{A}_{max}(w) \\ &\quad \times \exp \left[-\frac{(\mathbf{c}_{p1} - \mathbf{U}_p)^2 + (\mathbf{c}_{p2} - \mathbf{U}_p)^2}{2\Theta_p} \right] d\mathbf{w} d\mathbf{G}, \end{aligned} \quad (\text{A } 8)$$

where $\mathcal{A}_{max}(w)$ satisfies $\mathcal{A}_{max}(w) \cos^{4/5}(\theta') = \mathcal{A}_{max}(\mathbf{w} \cdot \mathbf{k})$; and Λ denotes the integral respect to \mathbf{k} and is given by

$$\Lambda = \int_0^{2\pi} \int_0^{\pi/2} \mathbf{k} \otimes \mathbf{k} \cos^{9/5} \theta' \sin \theta' d\theta' d\varphi' = \pi \begin{bmatrix} \frac{25}{168} & 0 & 0 \\ 0 & \frac{25}{168} & 0 \\ 0 & 0 & \frac{5}{12} \end{bmatrix}, \quad (\text{A } 9)$$

and \mathbf{R} is a rotation matrix representing rotation that transforms \mathbf{w} parallel to z -axis. The velocity coordinates can be expressed also in terms of spherical coordinates:

$$d\mathbf{w} = w^2 \sin \theta d\theta d\varphi dw, \quad (\text{A } 10)$$

and

$$d\mathbf{G} = 4\pi G^2 dG. \quad (\text{A } 11)$$

With the change of variables, the flux $\theta_1(q_p)$ becomes:

$$\begin{aligned} \theta_1(q_p) &= \frac{n_p^2}{(2\pi\Theta_p)^3} \mathbf{E}_{12} \cdot \int_0^{2\pi} \int_0^\pi \mathbf{R} \Lambda \mathbf{R}^T \sin \theta d\theta d\varphi \\ &\quad \times \int_0^\infty \mathcal{A}_{max}(w) \exp \left[-\frac{w^2}{4\Theta_p} \right] w^3 dw \\ &\quad \times \int_0^\infty 2\pi \exp \left[-\frac{G^2}{4\Theta_p} \right] G^2 dG. \end{aligned} \quad (\text{A } 12)$$

The first integral then becomes:

$$\int_0^{2\pi} \int_0^\pi \mathbf{R} \Lambda \mathbf{R}^T \sin \theta d\theta d\varphi = \frac{20}{21} \pi^2 \mathbf{I}, \quad (\text{A } 13)$$

where \mathbf{I} is identity tensor; the second integral is given by

$$\int_0^\infty \mathcal{A}_{max}(w) \exp \left[-\frac{w^2}{4\Theta_p} \right] w^3 dw = 2^{4/5} 16\pi \Gamma \left(\frac{12}{5} \right) r^* \left(\frac{15m_p}{32Y^* \sqrt{r^*}} \right)^{2/5} \Theta_p^{12/5}, \quad (\text{A } 14)$$

and the third integral evaluates as

$$\int_0^\infty 2\pi \exp \left[-\frac{G^2}{4\Theta_p} \right] G^2 dG = 4\pi \sqrt{\pi} \Theta_p^{3/2}. \quad (\text{A } 15)$$

Collecting the results from Eqs. (A 13), (A 14), and (A 15) to Eq. (A 12) leads to

$$\theta_1(q_p) = 40 \frac{2^{4/5} \pi \sqrt{\pi}}{21} n_p^2 \Gamma \left(\frac{12}{5} \right) r^* \left(\frac{15m_p}{32Y^* \sqrt{r^*}} \right)^{2/5} \Theta_p^{9/10} \mathbf{E}_{12}. \quad (\text{A } 16)$$

The second flux term in $\theta_2(q_p)$ can be simplified to

$$\begin{aligned}
\theta_2(q_p) &= \int_{\mathbf{w} \cdot \mathbf{k} > 0} \mathcal{A}_{max}(\mathbf{w} \cdot \mathbf{k}) (\mathbf{E}_{12}^+ \cdot \mathbf{k}) [\mathbf{w} \cdot \mathbf{k}] \mathbf{k} f_{p1} f_{p2} \mathbf{k} \cdot \nabla \ln \frac{f_{p2}}{f_{p1}} d\mathbf{k} d\mathbf{c}_{p1} d\mathbf{c}_{p2} dq_{p1} dq_{p2} \\
&= \int_{\mathbf{w} \cdot \mathbf{k} > 0} \mathcal{A}_{max}(\mathbf{w} \cdot \mathbf{k}) \left[\mathbf{E}_{12} \cdot \mathbf{k} + \frac{q_{p2} - q_{p1}}{\pi \varepsilon_0 d_p^2} \right] \\
&\quad \times [\mathbf{w} \cdot \mathbf{k}] \mathbf{k} f_{p1} f_{p2} \mathbf{k} \cdot \nabla \ln \frac{f_{p2}}{f_{p1}} d\mathbf{k} d\mathbf{c}_{p1} d\mathbf{c}_{p2} dq_{p1} dq_{p2} \\
&= \int_{\mathbf{w} \cdot \mathbf{k} > 0} \mathcal{A}_{max}(\mathbf{w} \cdot \mathbf{k}) (\mathbf{E}_{12} \cdot \mathbf{k}) \mathbf{k} [\mathbf{w} \cdot \mathbf{k}] f_{p1} f_{p2} \mathbf{k} \cdot \nabla \ln \frac{f_{p2}}{f_{p1}} d\mathbf{k} d\mathbf{c}_{p1} d\mathbf{c}_{p2} dq_{p1} dq_{p2} \\
&\quad + \int_{\mathbf{w} \cdot \mathbf{k} > 0} \mathcal{A}_{max}(\mathbf{w} \cdot \mathbf{k}) \frac{q_{p2} - q_{p1}}{\pi \varepsilon_0 d_p^2} [\mathbf{w} \cdot \mathbf{k}] \mathbf{k} f_{p1} f_{p2} \mathbf{k} \cdot \nabla \ln \frac{f_{p2}}{f_{p1}} d\mathbf{k} d\mathbf{c}_{p1} d\mathbf{c}_{p2} dq_{p1} dq_{p2} \\
&= \mathbf{E}_{12} \cdot \int_{\mathbf{w} \cdot \mathbf{k} > 0} \mathcal{A}_{max}(\mathbf{w} \cdot \mathbf{k}) [\mathbf{w} \cdot \mathbf{k}] f_{p1} f_{p2} (\mathbf{k} \otimes \mathbf{k} \otimes \mathbf{k}) \\
&\quad \cdot \nabla \ln \frac{f_{p2}}{f_{p1}} d\mathbf{k} d\mathbf{c}_{p1} d\mathbf{c}_{p2} dq_{p1} dq_{p2} \\
&\quad + \int_{\mathbf{w} \cdot \mathbf{k} > 0} \mathcal{A}_{max}(\mathbf{w} \cdot \mathbf{k}) \frac{q_{p2} - q_{p1}}{\pi \varepsilon_0 d_p^2} [\mathbf{w} \cdot \mathbf{k}] f_{p1} f_{p2} (\mathbf{k} \otimes \mathbf{k}) \\
&\quad \cdot \nabla \ln \frac{f_{p2}}{f_{p1}} d\mathbf{k} d\mathbf{c}_{p1} d\mathbf{c}_{p2} dq_{p1} dq_{p2}. \tag{A 17}
\end{aligned}$$

The first integral with the third rank tensor $\mathbf{k} \otimes \mathbf{k} \otimes \mathbf{k}$ vanishes since integration's over odd dimensional tensor are zero. Expanding the natural logarithm of particle density function ratios yields:

$$\nabla \ln \frac{f_{p2}}{f_{p1}} = \frac{1}{2Q_p^2} (q_{p2}^2 - q_{p1}^2) \nabla Q_p - \frac{1}{Q_p} (q_{p2} - q_{p1}) \nabla Q_p \tag{A 18}$$

$$+ \frac{1}{2\Theta_p^2} (c_{p2}^2 - c_{p1}^2) \nabla \Theta_p - \frac{1}{\Theta_p} \nabla \mathbf{U}_p \cdot (\mathbf{c}_{p2} - \mathbf{c}_{p1}). \tag{A 19}$$

As before, the integration's over the charge difference vanishes hence the third and fourth terms involving particle velocities integrate to zero. Hence, the second flux term becomes:

$$\begin{aligned}
\theta_2(q_p) &= \frac{n_p^2}{(2\pi\Theta)^3} \\
&\quad \times \int \frac{q_{p2} - q_{p1}}{\pi \varepsilon_0 d_p^2} \left(\frac{1}{2Q_p^2} (q_{p2}^2 - q_{p1}^2) \nabla Q_p - \frac{1}{Q_p} (q_{p2} - q_{p1}) \nabla Q_p \right) f_{p1,q} f_{p2,q} dq_{p1} dq_{p2} \\
&\quad \cdot \int_{\mathbf{w} \cdot \mathbf{k} > 0} (\mathbf{k} \otimes \mathbf{k}) \mathcal{A}_{max}(\mathbf{w} \cdot \mathbf{k}) [\mathbf{w} \cdot \mathbf{k}] \\
&\quad \times \exp \left[-\frac{(\mathbf{c}_{p1} - \mathbf{U}_p)^2 + (\mathbf{c}_{p2} - \mathbf{U}_p)^2}{2\Theta_p} \right] d\mathbf{k} d\mathbf{c}_{p1} d\mathbf{c}_{p2}, \tag{A 20}
\end{aligned}$$

where $f_{p1,q}$ and $f_{p2,q}$ denote normal distribution density functions of charge with mean Q_p and variance Q_p .

The velocity integral (same as I^v) can be evaluated in the same way as done for $\theta_1(q_p)$

and becomes:

$$\begin{aligned}
\Gamma^v &= \int_0^{2\pi} \int_0^\pi \mathbf{R} \Lambda \mathbf{R}^T \sin \theta d\theta d\varphi \\
&\quad \int_0^\infty \mathcal{A}_{max}(w) \exp\left[-\frac{w^2}{4\Theta_p}\right] w^3 dw \\
&\quad \int_0^\infty 2\pi \exp\left[-\frac{G^2}{4\Theta_p}\right] G^2 dG \\
&= \frac{20}{21} \pi^2 \mathbf{I} \\
&\quad \times 2^{4/5} 16\pi \Gamma\left(\frac{12}{5}\right) r^* \left(\frac{15m_p}{32Y^* \sqrt{r^*}}\right)^{2/5} \Theta_p^{12/5} \\
&\quad \times \pi \sqrt{\pi} \Theta_p^{3/2}. \tag{A 21}
\end{aligned}$$

The charge integration gives:

$$\int \frac{q_{p2} - q_{p1}}{\pi \varepsilon_0 d_p^2} \frac{1}{2Q_p^2} (q_{p2}^2 - q_{p1}^2) \nabla Q_p f_{p1,q} f_{p2,q} dq_{p1} dq_{p2} = \frac{2}{\pi \varepsilon_0 d_p^2} Q_p \nabla \ln Q_p \tag{A 22}$$

and

$$-\int \frac{q_{p2} - q_{p1}}{\pi \varepsilon_0 d_p^2} \frac{1}{Q_p} (q_{p2} - q_{p1}) \nabla Q_p f_{p1,q} f_{p2,q} dq_{p1} dq_{p2} = -\frac{2}{\pi \varepsilon_0 d_p^2} \nabla Q_p. \tag{A 23}$$

Finally, the second flux term becomes:

$$\theta_2(q_p) = \frac{5\sqrt{\pi}}{21} \frac{2^{9/10}}{d_p^2} n_p^2 \left(\Gamma\left(\frac{12}{5}\right) r^* \left(\frac{15m_p}{32Y^* \sqrt{r^*}}\right)^{2/5} \Theta_p^{9/10} \right) [Q_p \nabla \ln Q_p - \nabla Q_p]. \tag{A 24}$$

Appendix B. Discrete Element Modeling with Tribocharging

We simulated the motion of colliding particles using a time-driven approach with a hard sphere collision model. In the time-driven approach, we first predict particle positions at the beginning of the time-step by:

$$\mathbf{x}_i^{(n+1)*} = \mathbf{x}_i^{(n)} + \mathbf{c}_i^{(n)} \Delta t, \tag{B 1}$$

where Δt is the time step; $\mathbf{x}_i^{(n)}$ is the particle position at time $n\Delta t$; $\mathbf{c}_i^{(n)}$ is the particle velocity at time instant $n\Delta t$; and $\mathbf{x}_i^{(n+1)*}$ is the predicted particle location. If particles i and j overlap ($\|\mathbf{x}_i^{(n+1)*} - \mathbf{x}_j^{(n+1)*}\| < d_p$ where d_p is the particle diameter), the time is reversed for these two particles to first time of contact, $(n+f)\Delta t$, where $0 < f < 1$. Subsequently, particle velocities are updated according to hard sphere model:

$$\mathbf{c}_i^{(n+1)} = \mathbf{c}_i^{(n)} + \frac{1+e_c}{2} \left((\mathbf{c}_j^{(n)} - \mathbf{c}_i^{(n)}) \cdot \mathbf{n}_{ij} \right) \mathbf{n}_{ij}, \text{ and} \tag{B 2}$$

$$\mathbf{c}_j^{(n+1)} = \mathbf{c}_j^{(n)} - \frac{1+e_c}{2} \left((\mathbf{c}_j^{(n)} - \mathbf{c}_i^{(n)}) \cdot \mathbf{n}_{ij} \right) \mathbf{n}_{ij}, \tag{B 3}$$

where \mathbf{n}_{ij} is a unit vector pointing from particle i to particle j , and e_c is the restitution coefficient (e_c was set to 1 for DEM simulations). The particle position is then integrated from time $(n+f)\Delta t$ to the current time step $n+1$ with the updated velocities:

$$\mathbf{x}_i^{(n+1)} = \mathbf{x}_i^{(n)} + \mathbf{c}_i^{(n)} f \Delta t + \mathbf{c}_i^{(n+1)} (1-f) \Delta t. \tag{B 4}$$

The charge transfer during a collision given by Eq. (2.30) as:

$$\Delta q_{ij}^{(n)} = \frac{\beta_q}{\alpha_q} (1 - e^{-\alpha_q \mathcal{A}_{max}}). \quad (\text{B } 5)$$

The charges of the particles are then updated as

$$q_i^{(n+1)} = q_i^{(n)} - \Delta q_{ij}^{(n)}, \text{ and} \quad (\text{B } 6)$$

$$q_j^{(n+1)} = q_j^{(n)} + \Delta q_{ij}^{(n)}. \quad (\text{B } 7)$$

For wall collisions, the particle j is treated as an mirrored particle with the same charge as particle i and a work function difference $\Delta\varphi$ between them.

The electric field at a particle position was computed by a spectral method Eq. (B 8):

$$\mathbf{E}(\mathbf{x}) = \mathcal{F}^{-1} \left(\frac{\mathcal{F}(\rho(\mathbf{x}))}{\|\mathbf{k}\|^2} \mathbf{k} \right). \quad (\text{B } 8)$$

Here, the symbol \mathbf{k} is the vector wavenumber, ρ is the charge density, \mathcal{F} and \mathcal{F}^{-1} refer to the Fourier and inverse Fourier transforms, respectively. The charge density in any computational cell is related to charges of all the particles in that cell as $\rho = \frac{\sum_i^{cell} q_i}{V_{cell}}$ where V_{cell} is the volume of the computational cell.

REFERENCES

- AL-ADEL, M. F., SAVILLE, D. A. & SUNDARESAN, S. 2002 The effect of static electrification on gas-solid flows in vertical risers. *Industrial & Engineering Chemistry Research* **41** (25), 6224–6234.
- BENDIMERAD, S, TILMATINE, A, ZIANE, M & DASCALESCU, L 2009 Plastic wastes recovery using free-fall triboelectric separator. *International Journal of Environmental Studies* **66** (5), 529–538.
- BLISSETT, RS & ROWSON, NA 2012 A review of the multi-component utilisation of coal fly ash. *Fuel* **97**, 1–23.
- BOATENG, A. & BARR, P. 1996 A thermal model for the rotary kiln including heat transfer within the bed. *International Journal of Heat and Mass Transfer* **39** (10), 21312145–21432147.
- BOELLE, A., BALZER, G. & SIMONIN, O. 1995 Second-order prediction of the particle-phase stress tensor of inelastic spheres in simple shear dense suspensions. *ASME-PUBLICATIONS-FED* **228**, 9–18.
- CARTER, DYLAN & HARTZELL, CHRISTINE 2017 Extension of discrete tribocharging models to continuous size distributions. *Physical Review E* **95** (1), 012901.
- CERCIGNANI, C. 1975 *Theory and application of the Boltzmann equation*. Scottish Academic Press.
- CHEN, J. & HONAKER, R. 2015 Dry separation on coal-silica mixture using rotary triboelectrostatic separator. *Fuel Processing Technology* **131**, 317–324.
- CHOWDHURY, F, SOWINSKI, A, RAY, M, PASSALACQUA, A & MEHRANI, P 2018 Charge generation and saturation on polymer particles due to single and repeated particle-metal contacts. *Journal of Electrostatics* **91**, 9–15.
- DING, J. & GIDASPOW, D. 1990 A bubbling fluidization model using kinetic theory of granular flow. *AIChE Journal* **36** (4), 523–538.
- DUFF, N. & LACKS, D. J. 2008 Particle dynamics simulations of triboelectric charging in granular insulator systems. *Journal of Electrostatics* **66** (12), 51–57.
- FAN, F., TIAN, Z. & WANG, Z. L. 2012 Flexible triboelectric generator. *Nano Energy* **1** (2), 328–334.
- FÉVRIER, PIERRE, SIMONIN, OLIVIER & SQUIRES, KYLE D. 2005 Partitioning of particle velocities in gas-solid turbulent flows into a continuous field and a spatially uncorrelated random distribution: theoretical formalism and numerical study. *Journal of Fluid Mechanics* **533**, 1–46.

- FOTOVAT, F., ALSMARI, T. A., GRACE, J. R. & BI, X. T. 2016 The relationship between fluidized bed electrostatics and entrainment. *Powder Technology* .
- FOTOVAT, F., BI, X. T. & GRACE, J. 2017 Electrostatics in gas-solid fluidized beds: A review. *Chemical Engineering Science* **173**, 303–334.
- FOX, RODNEY O. 2014 On multiphase turbulence models for collisional fluidparticle flows. *Journal of Fluid Mechanics* **742**, 368–424.
- GARZÓ, V., TENNETI, S., SUBRAMANIAM, S. & HRENYA, C. M. 2012 Enskog kinetic theory for monodisperse gassolid flows. *Journal of Fluid Mechanics* **712**, 129–168.
- GATIGNOL, R. 1983 The Faxen formulas for a rigid particle in an unsteady non-uniform Stokes-flow. *Journal de Mecanique theorique et appliquee* **2** (2), 143–160.
- GOBIN, A., NEAU, H., SIMONIN, O., LLINAS, J., REILING, V. & SÉLO, J. 2003 Fluid dynamic numerical simulation of a gas phase polymerization reactor. *International Journal for Numerical Methods in Fluids* **43** (10-11), 1199–1220.
- GROSSHANS, H. & PAPALEXANDRIS, M. V. 2016 Large eddy simulation of triboelectric charging in pneumatic powder transport. *Powder Technology* **301**, 1008–1015.
- GROSSHANS, H. & PAPALEXANDRIS, M. V. 2017 Direct numerical simulation of triboelectric charging in particle-laden turbulent channel flows. *Journal of Fluid Mechanics* **818**, 465–491.
- GU, Z., WEI, W., SU, J. & YU, C. W. 2013 The role of water content in triboelectric charging of wind-blown sand. *Sci. Rep* **3** (1), 1337.
- HARPER, W. R. 1967 Contact and frictional electrification. PhD thesis, Oxford.
- HASSANI, M. A., ZARGHAMI, R., NOROUZI, H. R. & MOSTOUFI, N. 2013 Numerical investigation of effect of electrostatic forces on the hydrodynamics of gas–solid fluidized beds. *Powder Technology* **246**, 16–25.
- HENDRICKSON, G 2006 Electrostatics and gas phase fluidized bed polymerization reactor wall sheeting. *Chemical Engineering Science* **61** (4), 1041–1064.
- HOGUE, M. D., CALLE, C. I., WEITZMAN, P. S. & CURRY, D. R. 2008 Calculating the trajectories of triboelectrically charged particles using Discrete Element Modeling (DEM). *Journal of Electrostatics* **66** (12), 32–38.
- HSIAU, S. S. & HUNT, M. L. 1993 Kinetic theory analysis of flow-induced particle diffusion and thermal conduction in granular material flows. *Transactions-American Society of Mechanical Engineers Journal of Heat Transfer* **115**, 541–541.
- HUNT, M. 1997 Discrete element simulations for granular material flows: effective thermal conductivity and self-diffusivity. *International journal of heat and mass transfer* **40** (13), 3059–3068.
- JALALINEJAD, F, BI, XT & JR, GRACE 2016 Comparison of theory with experiment for single bubbles in charged fluidized particles. *Powder Technology* **290**, 27 – 32.
- JALALINEJAD, F., BI, X. T. & GRACE, J. R. 2015 Effect of electrostatics on interaction of bubble pairs in a fluidized bed. *Advanced Powder Technology* **26** (1), 329–334.
- JENKINS, J. T. & MANCINI, F. 1989 Kinetic theory for binary mixtures of smooth, nearly elastic spheres. *Physics of Fluids A: Fluid Dynamics* **1** (12), 2050–2057.
- JENKINS, J. T. & RICHMAN, M. W. 1985 Kinetic theory for plane flows of a dense gas of identical, rough, inelastic, circular disks. *Physics of Fluids (1958-1988)* **28** (12), 3485–3494.
- JENKINS, J. T. & RICHMAN, M. W. 1986 Grads 13-Moment System for a Dense Gas of Inelastic Spheres. In *The Breadth and Depth of Continuum Mechanics*, pp. 647–669. Springer Berlin Heidelberg.
- JENKINS, J. T. & SAVAGE, S. B. 1983 A Theory for the Rapid Flow of Identical, Smooth, Nearly Elastic, Spherical Particles. *Journal of Fluid Mechanics* **130**, 187–202.
- JONES, T. B. & KING, J. L. 1991 *Powder Handling and Electrostatics*. Lewis Publishers Inc.
- KARNIK, A. & SHRIMPTON, J. 2012 Mitigation of preferential concentration of small inertial particles in stationary isotropic turbulence using electrical and gravitational body forces. *Physics of Fluids* **24** (7), 073301.
- KIM, J., C., SOO S., HAN, S. W., LEE, K. H., KI, T. H., OH, J. Y., LEE, J. H., KIM, W. S., JANG, W. S. & BAIK, H. K. 2016 Triboelectric generator based on a moving charged bead. *Journal of Physics D: Applied Physics* **49** (47), 47LT02.
- KOCH, DONALD L. & SANGANI, ASHOK S. 1999 Particle pressure and marginal stability limits for

- a homogeneous monodisperse gas-fluidized bed: kinetic theory and numerical simulations. *Journal of Fluid Mechanics* **400**, 229–263.
- KOK, JF & LACKS, DJ 2009 Electrification of granular systems of identical insulators. *Physical Review E* **79** (5), 051304.
- KOLEHMAINEN, J., OZEL, A., BOYCE, C. M. & SUNDARESAN, S. 2016 A hybrid approach to computing electrostatic forces in fluidized beds of charged particles. *AIChE Journal* **62** (7), 2282–2295.
- KOLEHMAINEN, J., OZEL, A., BOYCE, C. M. & SUNDARESAN, S. 2017a Triboelectric charging of monodisperse particles in fluidized beds. *AIChE Journal* **63** (6), 1872–1891.
- KOLEHMAINEN, J., SIPPOLA, P., RAITANEN, O., OZEL, A., BOYCE, C.M., SAARENINNE, P. & SUNDARESAN, S. 2017b Effect of humidity on triboelectric charging in a vertically vibrated granular bed: Experiments and modeling. *Chemical Engineering Science* **173**, 363–373.
- KOREVAAR, M. W., PADDING, J. T., VAN DER HOEF, M. A. & KUIPERS, J. A. M. 2014 Integrated dem-cfd modeling of the contact charging of pneumatically conveyed powders. *Powder Technology* **258**, 144–156.
- LACKS, DJ & MOHAN, SR 2011 Contact electrification of insulating materials. *Journal of Physics D: Applied Physics* **44** (45), 453001.
- LAMARCHE, K. R., MUZZIO, F. J., SHINBROT, T. & GLASSER, B. J. 2010 Granular flow and dielectrophoresis: The effect of electrostatic forces on adhesion and flow of dielectric granular materials. *Powder Technology* **199** (2), 180–188.
- LAURENTIE, JC, TRAORÉ, P, DRAGAN, C & DASCALESCU, L 2010 Numerical Modeling of Triboelectric Charging of Granular Materials in Vibrated Beds. *Proceedings of Industry Applications Society Annual Meeting (IAS)* pp. 1–6.
- LAURENTIE, J. C., TRAORÉ, P. & DASCALESCU, L. 2013 Discrete element modeling of triboelectric charging of insulating materials in vibrated granular beds. *Journal of Electrostatics* **71** (6), 951–957.
- LEE, V, WAITUKAITIS, SR, MISKIN, MZ & JAEGER, HM 2015 Direct observation of particle interactions and clustering in charged granular streams. *Nature Physics* **11**, 733–737.
- LOWELL, J & ROSE-INNES, AC 1980 Contact electrification. *Advances in Physics* **29** (6), 947–1023.
- LUN, C. K. K. & SAVAGE, S. B. 1987 A simple kinetic theory for granular flow of rough, inelastic, spherical particles. *J. Appl. Mech* **54** (1), 47–53.
- LUN, C. K. K., SAVAGE, S. B., JEFFREY, D. J. & CHEPURNIY, N. 1984 Kinetic Theories for Granular Flow: Inelastic Particles in Couette Flow and Slightly Inelastic Particles in a General Flowfield. *Journal of Fluid Mechanics* **140**, 223–256.
- MATSUSAKA, S., MARUYAMA, H., MATSUYAMA, T. & GHADIRI, M. 2010 Triboelectric charging of powders: A review. *Chemical Engineering Science* **65** (22), 5781–5807.
- MATSUYAMA, T. & YAMAMOTO, H. 1995 Characterizing the electrostatic charging of polymer particles by impact charging experiments. *Advanced Powder Technology* **6** (3), 211–220.
- MAXEY, M. R. 1983 Equation of motion for a small rigid sphere in a nonuniform flow. *Physics of Fluids* **26** (4), 883.
- MCCARTY, L. S. & WHITESIDES, G. M. 2008 Electrostatic Charging Due to Separation of Ions at Interfaces: Contact Electrification of Ionic Electrets. *Angewandte Chemie International Edition* **47** (12), 2188–2207.
- MCCARTY, L. S., WINKLEMAN, A. & WHITESIDES, G. M. 2007 Ionic electrets: Electrostatic charging of surfaces by transferring mobile ions upon contact. *Journal of the American Chemical Society* **129** (13), 4075–4088.
- MEHROTRA, A., MUZZIO, F. J. & SHINBROT, T. 2007 Spontaneous separation of charged grains. *Physical review letters* **99** (5), 058001.
- MIZUTANI, M., YASUDA, M. & MATSUSAKA, S. 2015 Advanced characterization of particles triboelectrically charged by a two-stage system with vibrations and external electric fields. *Advanced Powder Technology* **26** (2), 454–461.
- NAIK, S, SARKAR, S, HANCOCK, B, ROWLAND, M, ABRAMOV, Y, YU, W & CHAUDHURI, B 2016 An experimental and numerical modeling study of tribocharging in pharmaceutical granular mixtures. *Powder Technology* pp. –.
- NAIK, S, SAURABH, S, VIPUL, G, BRUNO, HC, ABRAMOV, Y, YU, W & CHAUDHURI, B 2015 A combined experimental and numerical approach to explore tribocharging

- of pharmaceutical excipients in a hopper chute assembly. *International Journal of Pharmaceutics* **491**, 58–68.
- PÄHTZ, T, HERRMANN, HJ & SHINBROT, T 2010 Why do particle clouds generate electric charges? *Nature Physics* **6** (5), 364–368.
- PARK, A. & FAN, L. 2007 Electrostatic charging phenomenon in gasliquid-solid flow systems. *Chemical Engineering Science* **62** (12), 371–386.
- PEI, C, WU, CHUAN-YU, ENGLAND, D, BYARD, S, BERCHTOLD, H & ADAMS, M 2013 Numerical analysis of contact electrification using dem-cfd. *Powder Technology* **248**, 34–43.
- RAHMAN, M. A. & SAGHIR, M. Z. 2014 Thermodiffusion or soret effect: Historical review. *International Journal of Heat and Mass Transfer* **73**, 693–705.
- ROKKAM, RG, FOX, R & MUHLE, ME 2010 Cfd modeling of electrostatic forces in gas–solid fluidized beds. *The Journal of Computational Multiphase Flows* **2** (4), 189–205.
- ROKKAM, R. G., SOWINSKI, A., FOX, R. O., MEHRANI, P. & MUHLE, M. E. 2013 Computational and experimental study of electrostatics in gassolid polymerization fluidized beds. *Chemical Engineering Science* **92**, 146–156.
- SAKIZ, M. & SIMONIN, O. 1999 Development and validation of continuum particle wall boundary conditions using lagrangian simulation of a vertical gas-solid channel flow. In *Proc of FEDSM*, , vol. 99.
- SHELLA, A., HERMINGHAUS, S. & SCHRÖTER, M. 2016 Influence of humidity on the triboelectric charging and segregation in shaken granular media. *Soft Matter* .
- SCHILLER, L. & NAUMANN, Z. 1935 A drag coefficient correlation. *Vdi Zeitung* **77** (318), 51.
- SIU, THEO, COTTON, JAKE, MATTSON, GREGORY & SHINBROT, TROY 2014 Self-sustaining charging of identical colliding particles. *Physical Review E* **89** (5), 052208.
- SIU, THEO, PITTMAN, WILL, COTTON, JAKE & SHINBROT, TROY 2015 Nonlinear granular electrostatics. *Granular Matter* **17** (2), 165–175.
- SOWINSKI, ANDREW, MAYNE, ANTONIO & MEHRANI, POUPAK 2012 Effect of fluidizing particle size on electrostatic charge generation and reactor wall fouling in gassolid fluidized beds. *Chemical Engineering Science* **71**, 552–563.
- TAKADA, S., SAITOH, K. & HAYAKAWA, H. 2016 Kinetic theory for dilute cohesive granular gases with a square well potential. *Physical Review E* **94** (1), 012906.
- TANOUE, K., TANAKA, H., KITANO, H. & MASUDA, H. 2001 Numerical simulation of triboelectrification of particles in a gas–solids two-phase flow. *Powder technology* **118** (1), 121–129.
- WAITUKAITIS, S. R., LEE, V., PIERSON, J. M., FORMAN, S. L. & JAEGER, H. M. 2014 Size-dependent same-material tribocharging in insulating grains. *Physical Review Letters* **112** (21), 218001.
- WANG, Z. L. 2017 Catch wave power in floating nets. *Nature* **542** (7640), 159.
- WILES, J. A., FIALKOWSKI, M., RADOWSKI, M. R., WHITESIDES, G. M. & GRZYBOWSKI, B. A. 2004 Effects of Surface Modification and Moisture on the Rates of Charge Transfer between Metals and Organic Materials. *The Journal of Physical Chemistry B* **108** (52), 20296–20302.
- YANG, L. L., PADDING, J. T. & KUIPERS, J. A. M. 2016a Modification of kinetic theory of granular flow for frictional spheres, part i: Two-fluid model derivation and numerical implementation. *Chemical Engineering Science* **152**, 767–782.
- YANG, L. L., PADDING, J. T. & KUIPERS, J. A. M. 2016b Modification of kinetic theory of granular flow for frictional spheres, part ii: Model validation. *Chemical Engineering Science* **152**, 783–794.
- YANG, Y., GE, S., ZHOU, Y., SUN, J., HUANG, Z., WANG, J., LUNGU, M., LIAO, Z., JIANG, B. & YANG, Y. 2018 Effects of dc electric fields on meso-scale structures in electrostatic gas-solid fluidized beds. *Chemical Engineering Journal* **332**, 293–302.
- YANG, Y., ZI, C., HUANG, Z., WANG, J., LUNGU, M., LIAO, Z., YANG, Y. & SU, H. 2016c Cfd-dem investigation of particle elutriation with electrostatic effects in gas-solid fluidized beds. *Powder Technology* .
- YOSHIMATSU, R., ARAÚJO, N. A. M., SHINBROT, T. & HERRMANN, H. J. 2016 Field driven charging dynamics of a fluidized granular bed. *Soft matter* **12** (29), 6261–6267.

- YOSHIMATSU, R., ARAÚJO, N. A. M., SHINBROT, T. & HERRMANN, H. J. 2017*a* Segregation of charged particles in shear induced diffusion. *arXiv preprint arXiv:1705.04113* .
- YOSHIMATSU, R., ARAÚJO, N. A. M., WURM, G., HERRMANN, H. J. & SHINBROT, T. 2017*b* Self-charging of identical grains in the absence of an external field. *Scientific Reports* **7**.
- ZELMAT, M. E., RIZOUGA, M., TILMATINE, A., MEDLES, K., MILOUDI, M. & DASCALESCU, L. 2013 Experimental comparative study of different tribocharging devices for triboelectric separation of insulating particles. *IEEE Transactions on Industry Applications* **49** (3), 1113–1118.
- ZHOU, Y. S., WANG, S., YANG, Y., ZHU, G., NIU, S., LIN, Z., LIU, Y. & WANG, Z. L. 2014 Manipulating nanoscale contact electrification by an applied electric field. *Nano letters* **14** (3), 1567–1572.